International Journal of Heat and Mass Transfer 195 (2022) 123054

Contents lists available at ScienceDirect

International Journal of Heat and Mass Transfer

journal homepage: www.elsevier.com/locate/hmt

Universal Correlations for Post-CHF Saturated and Superheated Flow Film Boiling Heat Transfer Coefficient, Minimum Heat Flux and Rewet Temperature for Cryogenic Fluids in Uniformly Heated Tubes

Vishwanath Ganesan[a], Raj Patel[a], Jason Hartwig[b], Issam Mudawar[a,*]

[a] Purdue University Boiling and Two-Phase Flow Laboratory (PU-BTPFL), School of Mechanical Engineering, Purdue University, 585 Purdue Mall, West Lafayette, IN 47907, USA
[b] NASA Glenn Research Center, Fluids and Cryogenics Branch, Cleveland, OH 44135, USA

ARTICLE INFO

Article history:
Received 22 April 2022
Revised 17 May 2022
Accepted 18 May 2022
Available online 18 June 2022

Keywords:
Heat transfer coefficient
Film boiling
Inverted annular flow
Dispersed flow
Non-equilibrium
Actual quality
Minimum heat flux
Rewet temperature
Cryogens
Universal correlations

ABSTRACT

Despite the many experiments conducted throughout the globe during the past sixty years for a variety of cryogens to determine film boiling heat transfer coefficient (HTC) in a uniformly heated round tube, experimental data are either rarely published or published only for a few cryogens, with majority of the data remaining in archives of original authors, or in obscure technical reports of an organization or other inaccessible sources. In the present study, a very comprehensive data mining effort is undertaken to develop a consolidated database for Post Critical Heat Flux (CHF) flow boiling HTC for cryogens from world literature dating back to 1959. With 1730 local Dispersed Flow Film Boiling (DFFB) and 1310 local Inverted Annular Film boiling (IAFB) HTC data points for LHe, LH_2, LN_2, and LCH_4, it represents the largest cryogen post-CHF HTC database assembled to date. Using this database, new universal cryogen correlations for DFFB and IAFB HTCs are constructed and verified in terms of both predictive accuracy and trend. Similar efforts are carried out to collect a relatively small Minimum Heat Flux (MHF) and local Re-wet Temperature (RW) database, and construct correlations for both.

1. Introduction

1.1. Applications of Cryogenic Fluids

Cryogenic fluids are used in a broad range of industries. For example, in the food industry, Liquid Nitrogen (LN_2) is used to fast freeze food, whereas in the healthcare industry, it is used to preserve tissues and blood, and to destroy unhealthy tissues in cryosurgery. Liquid Oxygen (LOX) is also used in the healthcare industry especially in life support systems. Additionally, several cryogens, especially LOX, Liquid Hydrogen (LH_2), Liquid Methane (LCH_4), and Liquid Helium (LHe), have been used over the years in two primary applications: electronic cooling and space missions, the latter being the primary focus of the present study. In the field of electronic cooling, after an initial period of academic research interest in LHe heat transfer in West Germany [1], United States of America [2], and Japan [3,4] in the early 1970s, the decade of 1975–85 was a golden age for LHe flow boiling research in the Soviet Union in connection with development of forced convective cooling of superconducting systems [5–12]. Similar surge in LH_2 flow boiling research was observed in the decade post 2008 primarily in Japan, after a long gap with preliminary work done in the United States of America [13–15], with the objective of cooling large scale high temperature superconductor (HTS) magnets [16–25]. While LH_2 and LN_2 have been used over the years to cool high-temperature superconducting (HTS) magnets [16,26,27], LHe, having the lowest critical temperature of any known fluid, is also used to chill down Earth-orbiting telescopes and satellites as well as cool space experiments, where the ambient temperature in space is $\sim$ 2.7 K. And, following some initial work around 1960, LCH_4, received renewed interest in 2010 at NASA's Glenn Research Center [28] and Johnson Space Center [29–31] as part of their Propulsion and Cryogenics Advanced Development (PCAD) project, where nontoxic propellants such as LOX/LCH_4 were being tested for spacecraft applications. In nuclear thermal propulsion systems, LH_2 is used as a propellant, while LOX/LCH_4 or LOX/LH_2 are used in ascent stages, descent stages, and in-space fuel depots. LH_2 has also been proposed for future use as both propellent and coolant in several other advanced propulsion systems. Figure 1 shows examples of the space applications of cryogens.

* Corresponding author.
E-mail address: mudawar@ecn.purdue.edu (I. Mudawar).

https://doi.org/10.1016/j.ijheatmasstransfer.2022.123054
0017-9310/

Nomenclature

A	area
Bo	boiling number, q/Gh_{fg}
Bo^*	modified boiling number, $\frac{x_e - x_{e,in}}{1 - x_{e,in}}$
Bo^*_{MHF}	modified boiling number, $\frac{x_{e,MHF} - x_{e,in}}{1 - x_{e,in}}$, defined in Figure 19
c_p	specific heat at constant pressure
D	tube's inner diameter
Fr_{fo}	liquid-only Froude number, $\frac{G^2}{\rho_f^2 gD}$
$Fr_{g,D}$	vapor Froude number, $\frac{G}{\rho_{g,a}\sqrt{gD}}$
G	mass velocity
g	gravitational acceleration
h	local enthalpy, defined in Eq. (A1.1); heat transfer coefficient
h_a	local enthalpy defined using actual (non-equilibrium) quality, defined in Eq. (A1.4)
h_{DB}	heat transfer coefficient using the Dittus-Boelter formulation
h_e	local enthalpy defined using thermodynamic equilibrium quality, defined in Eq. (A1.3)
$h_{f,a}$	actual (non-equilibrium) enthalpy of liquid based on actual liquid temperature, $T_{f,a}$
$h_{f,e}$	saturated liquid enthalpy
h_{fg}	latent heat of vaporization
$h_{g,a}$	actual (non-equilibrium) enthalpy of vapor based on actual vapor temperature, $T_{g,a}$
$h_{g,e}$	saturated vapor enthalpy
$h_{tp,a}$	actual (non-equilibrium) two-phase heat transfer coefficient, $q/(T_w - T_{g,a})$
$h_{tp,DB,g,a}$	modified Dittus-Boelter correlation based on actual quality, x_a, and actual vapor temperature, $T_{g,a}$, defined in Eq. (6)
$h_{tp,e}$	equilibrium two-phase heat transfer coefficient, $q/(T_w - T_{g,e})$
$h_{tp,e,rewet}$	equilibrium two-phase heat transfer coefficient at MHF, $q/(T_{w,rewet} - T_{g,e})$
k	thermal conductivity
k_w	thermal conductivity of tube wall
L_H	heated length of tube
MAE	mean absolute error of any arbitrary term ϕ, $\frac{1}{N}\sum\frac{\lvert\phi_{pred}-\phi_{meas}\rvert}{\phi_{meas}} \times 100\%$
P	system pressure
$\Delta P_{max}/P$	maximum pressure drop ratio along the heated length of tube used by authors [91]
P_{crit}	critical pressure
P_R	reduced pressure, P/P_{crit}
$Pr_{g,a}$	actual vapor Prandtl number, $\mu_{g,a}\, c_{p,g,a}/k_{g,a}$
$Pr_{g,e}$	vapor Prandtl number, $\mu_{g,e}\, c_{p,g,e}/k_{g,e}$ if $0 \le x_e \le 1$ else $\mu_g\, c_{p,g}/k_g$
q	heat flux based on tube's inside area
$\dot{q}$	volumetric heat generation in tube wall
q_{CHF}	critical heat flux
q_{DNB}	critical heat flux for DNB type CHF mechanism
q_{MHF}	minimum heat flux
q_{max}	maximum heat flux post-CHF before decreasing it to eventually reach MHF
RMS	root mean squared error of any arbitrary term ϕ, $\sqrt{\frac{1}{N}\sum\left(\frac{\phi_{pred}-\phi_{meas}}{\phi_{meas}}\right)^2} \times 100\%$
$Re_{g,a}$	actual vapor Reynolds number, $GDx_a/\mu_{g,a}$
$Re_{g,e}$	vapor Reynolds number, $GDx_e/\mu_{g,e}$ if $0 \le x_e \le 1$ else GD/μ_g
S	slip ratio
T	local temperature
$\bar{T}$	average temperature
T_{crit}	critical temperature
$T_{f,a}$	actual (non-equilibrium) liquid temperature defined as $f(P, h_{f,a})$
$T_{g,a}$	actual (non-equilibrium) vapor temperature defined as $f(P, h_{g,a})$
$T_{g,e}$	equilibrium vapor temperature, equal to equilibrium liquid temperature, equal to equilibrium bulk fluid temperature defined as $f(P, h_e)$
T_λ	Lambda point temperature (2.17 K) for Liquid Helium transitioning from LHe I to LHe II
T_{sat}	saturation temperature
T_w	tube wall temperature
$T_{w,DB,g,a}$	tube wall temperature based on the Dittus-Boelter HTC formulation using $Re_{g,a}$, $Pr_{g,a}$ with all thermophysical properties evaluated at $T_{g,a}$, $T_{g,a} + \frac{q}{0.023 Re_{g,a}^{0.8} Pr_{g,a}^{0.4}\left(\frac{k_{g,a}}{d}\right)}$
$T_{w,DB,g,e}$	tube wall temperature based on the Dittus-Boelter HTC formulation using $Re_{g,e}$, $Pr_{g,e}$ with all thermophysical properties evaluated at $T_{g,e}$, $T_{g,e} + \frac{q}{0.023 Re_{g,e}^{0.8} Pr_{g,e}^{0.4}\left(\frac{k_{g,e}}{d}\right)}$
$T_{w,rewet}$	re-wet wall temperature at q_{MHF}
$\Delta T^*_{a,DB}$	normalized wall temperature w.r.t $T_{g,a}$, defined in Table 1
ΔT^*_{rewet}	normalized re-wet wall temperature at MHF, defined in Figure 19
$\Delta T^*_{sat,DB}$	normalized wall temperature w.r.t T_{sat}, defined in Eq. (8)
$\Delta T_{w,a}$	temperature difference between T_w and $T_{g,a}$
$\Delta T_{w,e}$	temperature difference between T_w and $T_{g,e}$
$\Delta T_{w,e,rewet}$	temperature difference between $T_{w.rewet}$ and $T_{g,e}$
t_w	tube wall thickness
u	mean velocity
$We_{fo,D}$	Weber number based on tube diameter, $G^2 D/(\rho_f \sigma)$
x_a	actual (non-equilibrium) quality
x_e	thermodynamic equilibrium quality
$x_{e,in}$	inlet thermodynamic equilibrium quality based on pressure at inlet of heated length, $(h_{in} - h_{f,in})/h_{fg,in}$
$x_{e,CHF}$	thermodynamic equilibrium quality at z_{CHF}
$x_{e,MHF}$	thermodynamic equilibrium quality at z_{MHF}
z	axial coordinate
z_{CHF}	axial location of CHF (DNB type or Dryout type) along the heated tube
z_{MHF}	axial location of MHF along the heated tube

Greek Symbols

α	void fraction
ε	tube surface roughness
θ	percentage of data points predicted within ±30%
μ	dynamic viscosity
ξ	percentage of data points predicted within ±50%
Π	dimensionless group
ρ	density
σ	surface tension

Subscripts

a	based on actual (non-equilibrium) quality, x_a

CHF	Critical Heat Flux
crit	critical point
DB	based on Dittus-Boelter formulation
DFFB	Dispersed Flow Film Boiling
DNB	Departure from Nucleate Boiling
e	based on thermodynamic equilibrium quality, x_e
exp	experimental (measured)
f	liquid
FB	Film Boiling
g	vapor
in	inlet
max	maximum
no-slip	assumes slip ratio, S, of unity
MHF	Minimum Heat Flux
NVG	Net Vapor Generation
ONB	Onset of Nucleate Boiling
RT	Re-Wet Temperature
pred	predicted
sat	saturated conditions
tp	two-phase
w	tube wall

Although almost all cryogens exist in unique states, LHe and LH_2 do not. LH_2 usually exists in two molecular spin states, orthohydrogen and parahydrogen, which exhibit significantly different thermal properties such as specific heat and thermal conductivity. Since the operating temperature of LH_2 for applications of interest to the present study is ~20.4 K, it is predominantly parahydrogen (0.2% ortho- and 99.8% para-) as compared to orthohydrogen (75% ortho- and 25% para) at 300 K. Similarly, LHe exists in two states, LHe I (at temperatures greater than the lambda temperature, T_λ) and LHe II (at temperatures lower than T_λ). Since the operating temperature of LHe for applications of interest to the present study is greater than 2.17 K, all the LHe data examined correspond to LHe I. From here on, both liquid parahydrogen and liquid helium I will be referred to as LH_2 and LHe, respectively.

1.2. Experimental Issues Unique to Post-CHF Region for Cryogens

Cryogens constitute a unique class of fluids which are clearly distinguishable from water and refrigerants by virtue of their low saturation temperatures, as shown in Fig. 2 (calculated using REFPROP 10 [32]). Owing to these low temperatures, cryogens are highly susceptible to liquid-to-vapor phase change – boiling – in most space applications of interest. While different boiling schemes (e.g., micro-channel [33] and jet impingement [34]) and fluid enhancement methods [35,36] are known to alter heat transfer performance, boiling configuration in most space applications is one of simple flow boiling in tubes. Four unique issues associated with cryogenic flow boiling which otherwise are often neglected when working with fluids at room temperature and terrestrial gravity are test section material selection, wall temperature and/or bulk vapor temperatures exceeding critical temperature, and reduced gravity effects [37].

1.2.1. Test section material

In most flow boiling experiments, the test section wall is subjected to external heating so that the fluid inside the test section is subjected to uniform heat flux both circumferentially and axially. However, owing to high heat flux conditions required to establish stable film boiling (Post-DNB), for test sections employing resistive heating, heat flux along the heated test section tends to be non-uniform [38,39]. This is primarily due to dependence of resistivity of the heating element on temperature. Figure 3 shows a comparison of wall thermal conductivities (calculated using EES 10 [40]) for commonly used test section materials, evaluated at critical temperature for cryogens. From the plot, it is evident that copper and silver must be avoided as test section materials for cryogenic experiments.

1.2.2. Wall and/or bulk vapor temperature exceeding critical temperature

Due to low critical temperatures of cryogens as opposed to common fluids, both the wall and the equilibrium bulk vapor temperature often exceed the critical temperature, as will be shown and discussed in later sections. Figure 4 shows variations of the relative difference in thermophysical properties of vapor, evaluated at the critical temperature, from that at saturation temperature, with reduced pressure. Figures 4(a) and 4(b) show excessively high differences in vapor densities and vapor viscosities, respectively, for both LHe and LH_2, whereas other cryogens show trends closer to those of common fluids. Figures 4(c) and 4(d) show variations of vapor specific heat and thermal conductivity, respectively: no anomalous behavior is observed here for cryogens.

1.2.3. Post-CHF flow boiling regimes

Post-CHF flow film boiling can take one of two forms based on the dominant CHF mechanism. For *DNB-Type CHF, Inverted Annular Flow Film Boiling (IAFB)* is observed first, which is comprised of a liquid core surrounded by a vapor film covering the test section's inner wall. This flow regime continues to manifest until the flow enters a *transition region* wherein the evaporating liquid core breaks down due to capillary interfacial waves or inertially due to fluctuating flow rate. This transition region, often referred to as "inverted slug" [41], is comprised of relatively large liquid slugs which continue to exist until they eventually break down into small liquid droplets dispersed both across and along the test section in a vapor continuum, described as *Dispersed Flow Film Boiling (DFFB).* For *Dryout-Type CHF,* however, only DFFB is encountered and persists until the dispersed liquid droplets are completely evaporated. Figure 5 shows schematics comparing the two distinct film boiling mechanisms based on CHF type.

1.3. Inverted Annular Film Boiling (IAFB)

In the IAFB regime, the liquid phase is present in the core of the heated test section forming a subcooled liquid core ('jet'), which is surrounded by an annular layer of saturated or superheated vapor. The test section is subjected to external heating which warms both the vapor layer and liquid core. Gradual evaporation of the liquid core both decreases the core diameter and increases velocity of the vapor layer, which typically becomes turbulent. The large velocity difference between the vapor and liquid culminates in interfacial waves which eventually grow unstable. Large amplitude of the unstable interface begins to break the liquid core, first to liquid slugs and farther downstream, because of continued evaporation, into small liquid droplets that are dispersed in saturated or superheated vapor.

Two distinct correlations have been proposed for prediction of heat transfer coefficient in the IAFB regime: modified McAdams-type [42] and Bromley-type [43]. The McAdams [42] correlation is expressed as

$$h_{tp,a} = c_1 Re_{g,a}^{c_2} Pr_{g,a}^{c_3} \frac{k_{g,a}}{D} \Pi(x_a), \tag{1}$$

which is based on Reynolds and Prandtl numbers of vapor corresponding to actual vapor conditions in the inverted annular film, and a dimensionless function Π of *actual vapor quality,* x_a (to be discussed in a subsequent section), with empirical constants c_1, c_2, and c_3 fitted using experimental IAFB data. Whereas, the Bromley-type [43] correlation, which is valid for $Fr_{g,D} > 2$, is expressed as

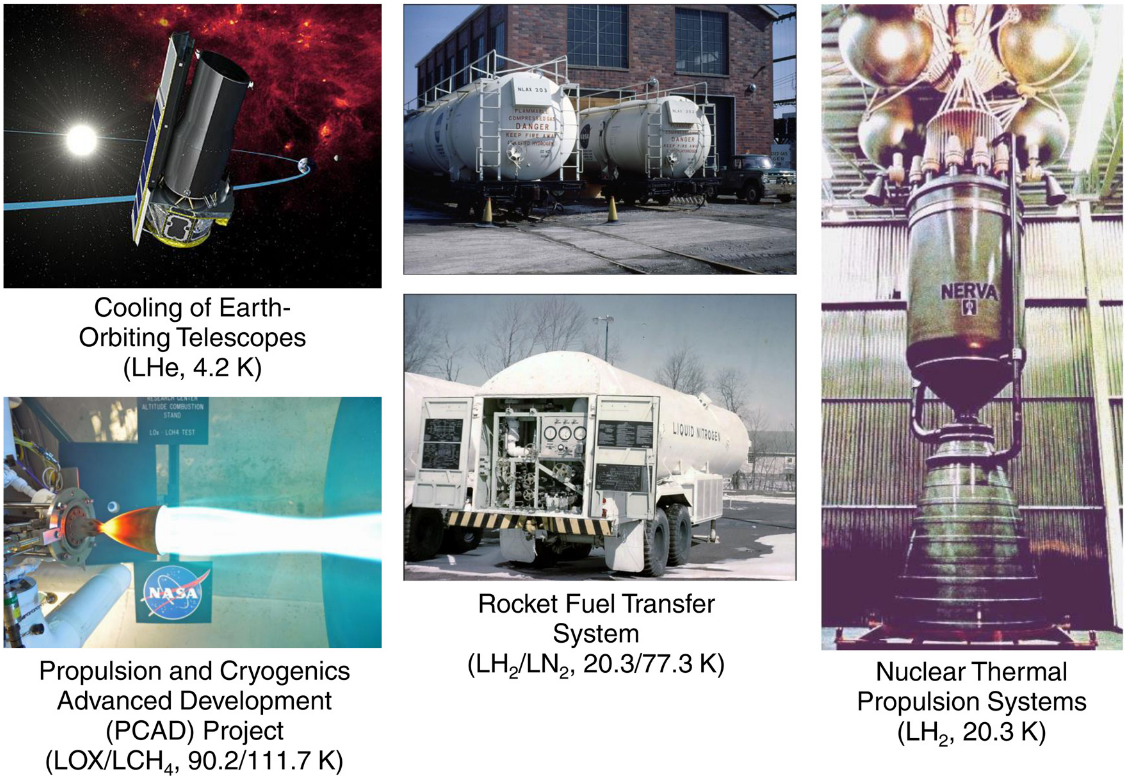

Fig. 1. Examples of space applications of cryogens.

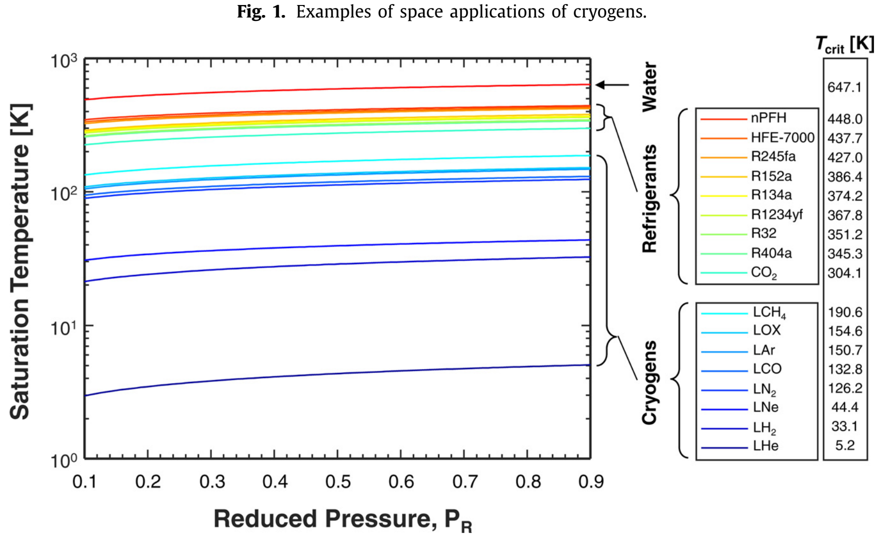

Fig. 2. Classification of coolants into water, refrigerants, and cryogens based on variation of saturation temperature with reduced pressure.

$$h_{tp,a} = c_1 \sqrt{\frac{k_{g,a}\rho_{g,a}h_{fg}\left(1 + \frac{0.4c_{p,g,a}(T_w - T_{sat})}{h_{fg}}\right)^2}{(T_w - T_{sat})}\Pi\left(Fr_{g,D}\right)}\sqrt{\frac{g}{D}} \quad (2)$$

where the dimensionless group Π is a function of vapor Froude number, $Fr_{g,D}$, and empirical constant $c_1 = 2.7$ is fitted using experimental IAFB data.

In the current study, a correlation for the cryogenic saturated and superheated IAFB will be developed using the McAdams-type correlation [42], which is easier to work with.

1.4. Dispersed Flow Film Boiling (DFFB)

As seen in Fig. 5, the DFFB regime can occur in both DNB-type and Dryout-type CHF situations. In this regime liquid droplets are dispersed in a vapor continuum along a heated test section. Given their small thermal mass, the liquid droplets maintain saturation temperature while the vapor is being gradually superheated. This can lead to appreciable thermodynamic non-equilibrium across the flow area. Some of the prior correlations for heat transfer coefficient in the DFFB regime (*e.g.*, Dougall [44], Groeneveld [45]) relied on the assumption of equilibrium flow, rendering them invalid for regions with strong non-equilibrium. But subsequent mechanistic models, such as those by Laverty and Rohsenow [46], Forslund and Rohsenow [47], Hynek [48], and Varone and Rohsenow [49], did take into account non-equilibrium effects as well as drag on liquid droplets. Unfortunately, use of these models is complicated by reliance on a system of equations containing a high degree of empiricism. More recently, Shah [50] proposed a correlation for two-phase heat transfer coefficient in the DFFB regime which both

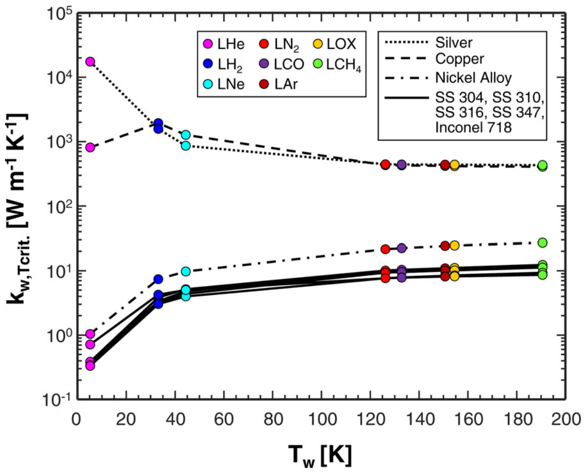

Fig. 3. Variation of thermal conductivity for commonly used wall materials with wall temperature corresponding to critical temperatures for cryogens.

takes non-equilibrium effects into account and is simple to use. In the present study, the functional form proposed by Shah [50] is adopted as basis for development of a new correlation for saturated and superheated cryogenic DFFB.

1.5. Fluid Physics Unique to Non-Equilibrium in DFFB

A key aspect of the afore-mentioned non-equilibrium effects in DFFB is that the heat supplied to the test section goes far more to heating the vapor than evaporating the liquid. As the small dispersed droplets undergo gradual evaporation, the liquid can be approximated as maintaining saturation temperature, whereas the vapor temperature maintains "*actual vapor temperature,*" $T_{g,a}$, that exceeds the "*equilibrium bulk temperature,*" $T_{g,e}$,; the latter being calculated using a simple thermodynamic energy balance. Figure 6(a) - 6(c) shows variations of wall temperature, vapor temperature, heat transfer coefficient, and vapor quality along with schematics of flow regime development for DFFB in a uniformly heated tube with subcooled, saturated liquid, and two-phase mixture inlet conditions, respectively.

In DFFB, the liquid can be assumed to maintain saturated state, thus allowing evaluation of actual vapor enthalpy, $h_{g,a}$, as (see Appendix 1 for details)

$$h_{g,a} = h_{g,e} + \left(\frac{x_e - x_a}{x_a}\right) h_{fg}, \tag{3}$$

where x_e and x_a are the thermodynamic equilibrium quality and actual non-equilibrium quality, respectively. The actual quality is defined as ratio of vapor to total mass flow rate,

$$x_a = \frac{\rho_{g,a} u_{g,a} A_{g,a}}{\rho_{g,a} u_{g,a} A_{g,a} + \rho_f u_f A_f} = \frac{1}{1 + \left[\frac{\rho_f}{\rho_{g,a}} \frac{1}{S} \left(\frac{1-\alpha}{\alpha}\right)\right]}, \tag{4}$$

where $u_{g,a}$, $u_{f,a}$, $A_{g,a}$, and $A_{f,a}$ are flow parameters representing mean vapor velocity, liquid velocity, vapor flow area, and liquid flow area, respectively, and S is slip ratio defined as $u_{g,a}/u_{f,a}$. Based on the approximation of well dispersed flow for post-CHF DFFB, a slip ratio of unity is assumed, which simplifies Eq. (4) to yield the following relation for local void fraction,

$$\alpha_{no-slip} = \frac{x_a \rho_f}{(1 - x_a)\rho_{g,a} + x_a \rho_f}. \tag{5}$$

Forslund and Rohsenow [39] reported experimentally determined, albeit sparse, actual quality values for LN_2, which was measured using the helium tracer gas technique. The parameter ranges for their saturated/superheated DFFB database are provided in Table 1. Figure 7(a) shows that majority of these datapoints have actual vapor temperature exceeding the critical temperature.

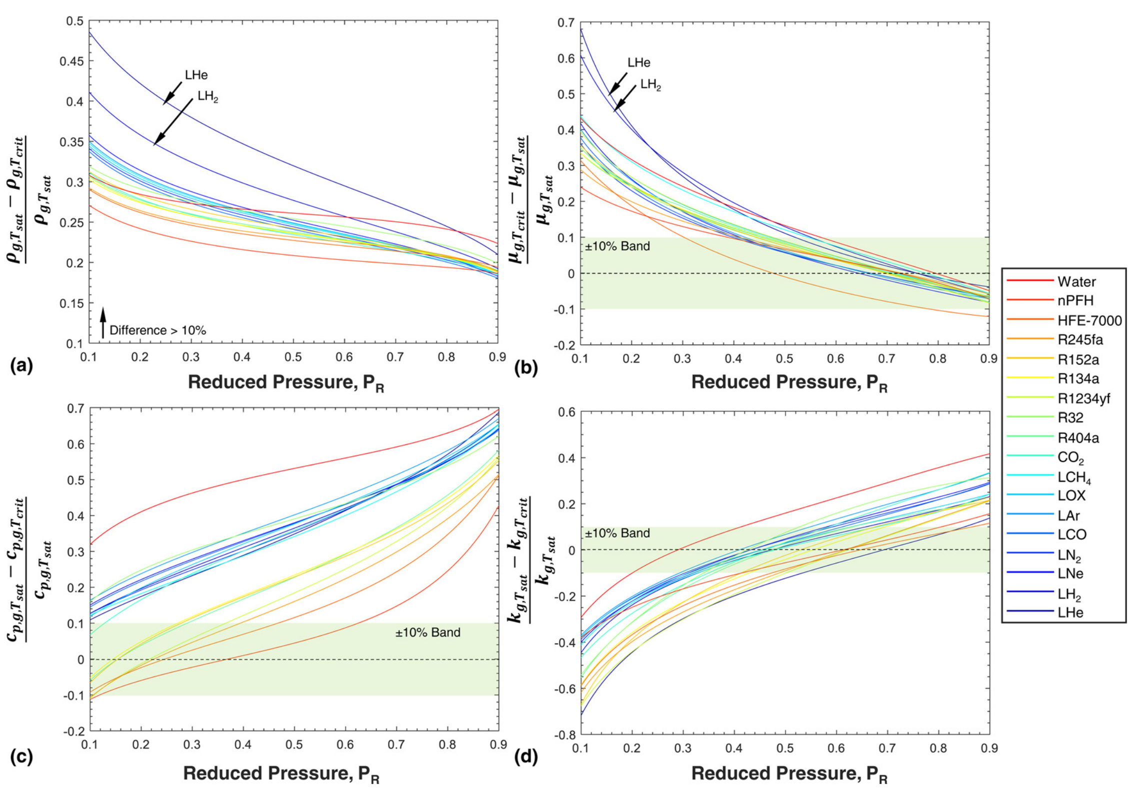

Fig. 4. Variations of relative difference in (a) vapor density, (b) vapor viscosity, (c) vapor specific heat, and (d) vapor thermal conductivity, evaluated at critical temperature from that at saturation temperature, with reduced pressure for cryogens compared to those of other fluid classes.

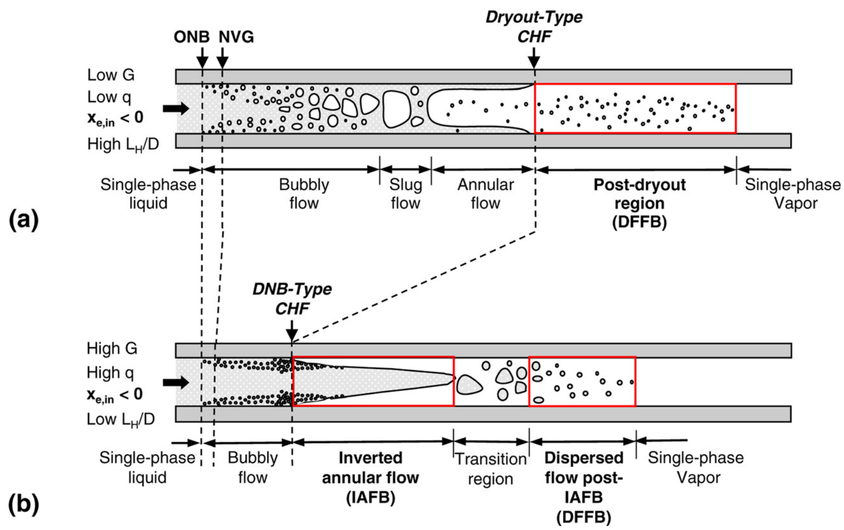

Fig. 5. Schematics comparing flow pattern development and film boiling regimes along a uniformly heated tube in vertical upflow with subcooled inlet for (a) Dryout-type CHF and (b) DNB-type CHF.

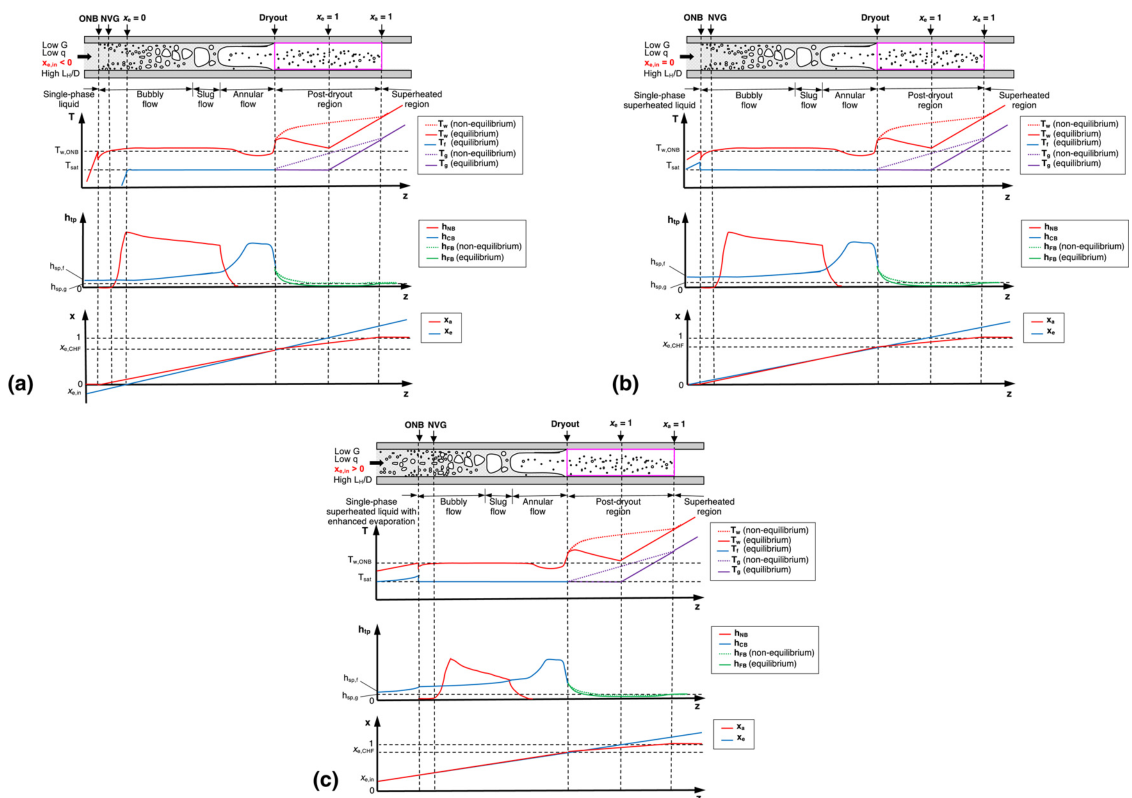

Fig. 6. Schematics of flow regime development and axial variations of vapor temperature, wall temperature, two-phase heat transfer coefficient, and vapor quality along uniformly heated tube undergoing DFFB (highlighted region) in vertical upflow for Dryout-type CHF with (a) subcooled inlet (b) saturated liquid inlet, and (c) two-phase mixture inlet.

Figure 7(b) also confirms that, even if equilibrium vapor temperature is smaller than critical temperature, the actual vapor temperature can be greater than the critical temperature due to non-equilibrium effects.

1.6. Objectives of Present Study

The present study is motivated by the lack of a large, reliable, error-free cryogen post-CHF heat transfer coefficient (HTC) database that can be used for developing correlations and mechanistic models to predict HTC in saturated and superheated flow film boiling. Another motivation is the lack of a simple, accurate, 'universal' film boiling HTC correlation for cryogenic flow in a uniformly heated tube.

Following are key objectives of the present study:

(1) Amass cryogenic flow film boiling HTC databases available from world literature for uniformly heated tubes.
(2) Carefully assess the accumulated data on a point-by-point basis to exclude any inaccurate data or data missing vital information, such as operating conditions, and apply systematic criteria for data exclusions.

Table 1
Parameter ranges for experimentally determined actual (non-equilibrium) quality for post-CHF saturated/superheated dispersed flow film boiling (DFFB) data for LN_2.

Reference	Acceptable x_a data	Tube dimensions		Operating and Inlet Conditions				Local Equilibrium and Non-equilibrium Conditions [b,c,d]						Remarks
		$D \times 10^3$ [m]	L_H/D	$P \times 10^{-6}$ [N m^{-2}]	G [kg m^{-2} s^{-1}]	$q \times 10^{-3}$ [W m^{-2}]	$x_{e,in}$	x_e	x_a	x_a/x_e	$T_{g,a}/T_{g,e}$	$\Delta T^*_{a,DB}$	$\alpha_{no\text{-}slip}$	
Forslund and Rohsenow [*,a] [39]	75	5.8 11.7	148.61 421.05	0.17 0.18	92.65 259.98	16.48 76.82	−0.06 0	0.25 2.95	0.21 1.00	0.33 1.00	1.00 2.59	1.07 1.34	0.98 1.00	SS 304 Tube t_w = 0.51 – 1.07 mm CHF type [e]: DNB Flow Regime [f]: DFFB (*post*-IAFB)

[*] Actual quality, x_a, found experimentally for LN_2 vertical upflow data using helium tracer gas technique.
[a] 4 data points with $T_{g,a} < T_{g,e}$ rejected due to energy balance violation
1 data point with $T_{g,a} > T_w$ rejected due to heat transfer violation
1 data point with $\Delta T^*_{a,DB} = 0.42 << 1$ rejected due to dispersed flow film boiling physics violation ($T_w < T_{w,DB,g,a}$).
[b] $T_{g,a} = f(P, h_{g,a})$, where $h_{g,a}$ is evaluated using Eq. (3).
[c] $\Delta T^*_{a,DB}$ is defined as $\frac{T_w - T_{g,a}}{T_{w,DB,g,a} - T_{g,a}}$, where $T_{w,DB,g,a} = T_{g,a} + \frac{q}{0.023 Re_{g,a}^{0.8} Pr_{g,a}^{0.4} \left(\frac{k_{g,a}}{d}\right)}$.
[d] $\alpha_{no\text{-}slip}$ for dispersed flow (assuming slip ratio, S, of unity) is defined using Eq. (5).
[e] All data in this reference are associated with non-uniform heat flux conditions due to strong axial conduction, leading to strong axial variation in wall temperature and therefore electrical resistance. Hence, CHF type identified from the original source [39]. It is reported that DNB (burnout) occurs at the entrance of the test section.
[f] Film boiling flow regime, dependent on CHF type, is identified from the original source [39].

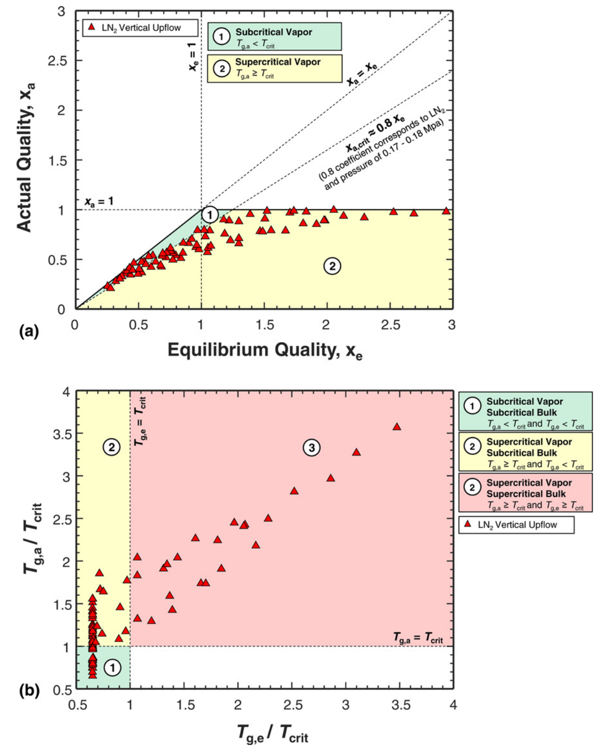

Fig. 7. Variations of (a) experimentally determined actual quality, x_a, with thermodynamic equilibrium quality, x_e, and (b) corresponding ratio of actual vapor temperature, $T_{g,a}$, and equilibrium vapor temperature, $T_{g,e}$, to critical temperature, T_{crit}, for LN_2 vertical upflow DFFB data obtained by Forslund and Rohsenow [39].

(3) Compile a new Purdue University Boiling and Two-Phase Flow Laboratory (PU-BTPFL) post-CHF Cryogenic HTC Database after applying the data exclusions.
(4) Carefully segregate the Database based on cryogen (LHe, LH_2, LN_2, and LCH_4) and flow orientation (vertical upflow, vertical downflow, and horizontal flow).
(5) Develop a classifier to segregate IAFB from DFFB data.
(6) Using the Database, develop a new “Universal DFFB Cryogenic HTC Correlation” for both saturated and superheated local conditions.
(7) Using the Database, develop a new “Universal IAFB Cryogenic HTC Correlation” for both saturated and superheated local conditions.
(8) Develop new correlations for Minimum Heat Flux (MHF) and local Rewet Temperature (RT).
(9) Identify ‘gaps’ in available post-CHF cryogenic HTC data that warrant future experimental investigation.
(10) Recommend a methodology for acquiring future post-CHF cryogenic HTC data in a manner that is conducive to refining HTC correlations and/or mechanistic models.

2. Compilation of Cryogen Post-CHF Flow Film Boiling HTC

As indicated earlier, the present study involved exhaustive data mining of post-CHF saturated and superheated boiling cryogenic HTC data from all literature sources available to the present authors. This included (1) major cryogen journals (*e.g.,* Cryogenics (Elsevier) and Advances in Cryogenic Engineering (Springer)), (2) major cryogen conferences (*e.g.,* International Cryogenic Engineering Conference and Cryogenic Engineering Conference (early papers published in Advances in Cryogenic Engineering)), (3) NASA and NIST technical reports, and (4) other sporadic publications, reports and theses from across the globe.

Only local HTC data with clearly prescribed inlet conditions, *i.e,* $h_{tp} = f(q, P_{in}, D, G, x_{e,in}, z)$ are considered in this study. Unless HTC data are explicitly specified in a given reference, the data is generated from plots of wall temperature distribution along the heated test section for a given heat flux. Additionally, any datapoint missing either heat flux or flow quality information is rejected.

The data mining effort was complicated by difficulty acquiring certain references because of such factors as (a) lack of availability from international interlibrary services, (b) reluctance of a few investigators to share their own database, and (c) lack of English translated versions of foreign literature with data. Avoidance of duplicate data was a thorough and time-consuming effort, necessitated by the fact that many published works lacked clear indication of sources for the data presented. Overall, data duplication in the HTC database was avoided by careful point-by-point inspection of the acquired data.

After completing the initial data mining effort and making certain of absence of duplicate data, efforts shifted to excluding data that did not strictly conform to the following uniformity requirements:

(1) Only single-component cryogens; data for binary or higher order mixtures are excluded.
(2) Only flow boiling in tubes; data for boiling in capillary tubes, thermosyphons, and natural circulation two-phase flows are excluded.
(3) Flow in only straight circular tubes; data for non-circular test sections (*e.g.,* rectangular, square, annular, rod, or bundles), helical tubes or U-bends are excluded.
(4) Flow in only stationary tubes; data for rotating tubes are excluded.
(5) Flow not involving use of swirl flow promotor (*e.g.,* twisted tape or wire coil insert) within the tube or upstream of the tube's inlet.
(6) Flow not involving use of abnormal test section inlet or outlet (*e.g.,* orifice plate, inlet expansion, or outlet expansion).
(7) Flow in tubes whose inner walls are not modified (*e.g.,* finned) for the purpose of enhancing heat transfer performance.
(8) Flow in tubes whose inner walls are not altered for the purpose of enhancing nucleation.
(9) Only data for vertical upflow, vertical downflow, and horizontal flow; data for inclined tubes are excluded.
(10) Only steady state data; transient boiling data are excluded.
(11) Only fully wetted tube data; horizontal flow boiling data for stratified and stratified-wavy flow regimes are excluded.
(12) Only HTC data presented by original authors with documented values for every parameter necessary for correlating the data (*e.g.,* heat flux, operating pressure, mass velocity, local quality, tube geometry, axial location, *etc.*) are considered.

This exclusion strategy, summarized in Table 2 , resulted in an initial database suitable for developing correlations (also future models) for post-CHF saturated and superheated flow boiling cryogenic HTC data.

3. Post-CHF HTC Correlation

As seen from Figs. 5 and 6, dispersed flow film boiling is identifiable in the high x_e range including the superheated non-equilibrium region between $x_e = 1$ and $x_a = 1$. In pursuit of new correlations for film boiling, this study will focus first on developing a new heat transfer coefficient correlation for cryogenic DFFB using high x_e data values and transition thereafter to correlations for low x_e data.

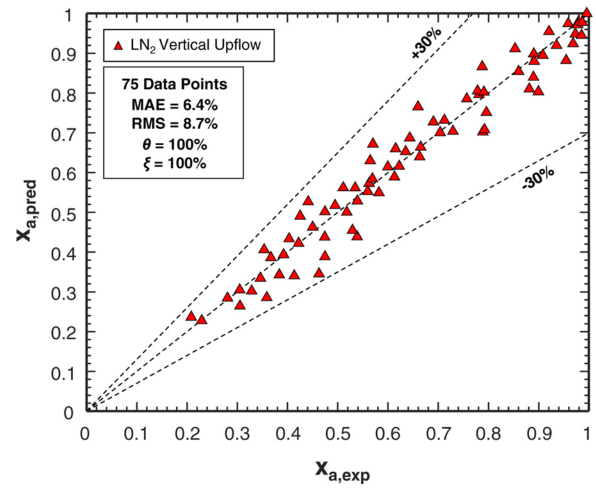

Fig. 8. Comparison of predicted actual quality, x_a, using the new correlation for post-CHF saturated and superheated DFFB for LN_2 vertical upflow and DFFB data obtained by Forslund and Rohsenow [39].

3.1. Universal Actual Quality Correlation

Using the experimentally determined actual quality data by Forslund and Rohsenow [39], Table 1, a correlation for actual quality is developed for both saturated and superheated post-CHF LN_2 DFFB data as detailed in Table 3 and shown graphically in Fig. 8. The functional form adopted in developing this correlation is based on Shah [50]. Although the correlation is developed for LN_2 vertical upflow DFFB data, it will be later shown the empirical constants in this correlation do not vary for other cryogenic fluids and flow orientations undergoing DFFB.

3.2. Universal HTC Correlation Methodology

Owing to strong non-equilibrium effects associated with DFFB, it is imperative to understand the importance of reference temperature in the definition of experimental heat transfer coefficient. Figure 9 compares this difference by defining the experimental two-phase HTC using both equilibrium vapor temperature, $T_{g,e}$, Fig. 9(a), and actual vapor temperature, $T_{g,a}$, Fig. 9(b), and plotting results against HTC predicted for LN_2 DFFB data by Forslund and Rohsenow [39] using the modified form of Dittus and Boelter [90] correlation based on actual quality, x_a,

$$h_{tp,DB,g,a} = 0.023 Re_{g,a}^{0.8} Pr_{g,a}^{0.4} \frac{k_{g,a}}{D}, \tag{6}$$

where experimentally obtained x_a information is available in Table 1. Clearly, when using correlations based on actual quality (to capture the non-equilibrium effects), better agreement between predicted and experimental values is achieved by using actual vapor temperature, $T_{g,a}$, as opposed to equilibrium vapor temperature, $T_{g,e}$, as reference temperature. For saturated DFFB and superheated DFFB, $T_{g,e} = T_{sat}$ and $T_{g,e} = f(P,h_e)$, respectively.

Before developing individual universal HTC correlations, it is important to first distinguish data for each of the two post-CHF regimes of DFFB versus IAFB. Figure 10 uses the saturated and superheated LN_2 DFFB data by Forslund and Rohsenow [39] to test trends against two classifiers: (i) modified boiling number, Bo^*, and (ii) normalized wall temperature, $\Delta T^*_{sat,DB}$, where

$$Bo^* = \frac{x_e - x_{e,in}}{1 - x_{e,in}} = \frac{4Bo}{1 - x_{e,in}} \frac{z}{D}, \tag{7}$$

Table 2
Data exclusion strategy for single component post-CHF HTC data for sub-critical cryogenic flow boiling in uniformly heated straight circular tubes.

Reference	Deviation from standard flow configuration [a]	Missing data	Miscellaneous factors	Remarks
(a) Complete Exclusion				
Monroe et al. [51]		•		Inlet quality information missing; exact test section length not specified
Dean and Thompson [52]	•			Annular circular test section with heater in the core
von Glahn and Lewis [38]	•	•		Non-uniform heat flux in test section due to strong wall temperature dependence on electrical resistance heating; only overall range for pressure provided for certain data points and inlet quality information missing
Walters [53]		•	•	Duplicate data from Wright & Walters [14]; only overall range for mass velocity provided
Jones and Altman [54]	•			Circular test section with U-bend
Burke and Rawdon [55]	•	•		Thermal capacitor rings used as heat source; heat flux information missing for certain data points; only overall range for inlet quality provided; certain tests performed with twisted tapes
Forslund and Rohsenow [39]	•			Non-uniform heat flux in test section due to strong wall temperature dependence on electrical resistance heating
Jergel & Stevenson [56]	•			Free convection laminar flow in rectangular channel test section with only a small fraction of test section heated
Bergles et al. [57]	•	•	•	Certain tests performed using twisted tape inserts to generate swirl flow; duplicate data from Hynek et al. [48]; inlet quality information missing for certain data points
Bergles et al. [58]	•	•	•	Certain tests performed using twisted tape inserts to generate swirl flow; duplicate data from Hynek et al. [48]; inlet quality information missing for certain data points
Iloeje et al. [59]	•			Tests performed under non-uniform heat flux conditions
Jones and Johnson [60]		•	•	Duplicate data in Giarratano et al. [61]; only overall range for inlet quality provided for certain data points
Grigoriev et al. [62]			•	Film boiling data indistinguishable from transition boiling (*"critical flow regime"*) data
Mohr and Runge [63]		•		Inlet quality information missing
Kurilenko and Dymenko [64]		•		Experimental data provided only in the form of dimensionless groups
Petukhov et al. [65]		•		Only overall range for mass velocity provided for certain data points; inlet quality information missing
Klimenko et al. [66]		•	•	Mass velocity and heat flux information missing for certain data points; horizontal flow boiling in stratified flow regime [d]
Roman and Karr [67]		•		No information provided about operating conditions
Bredy *et al.* [68]			•	Horizontal flow boiling in stratified flow regime [d]
Panek et al. [69]			•	Only transition boiling data post CHF provided
Umekawa & Ozawa [70]	•			Natural circulation driven two-phase flow in closed loop
Benkheria et al. [71]	•			Thermosyphon two-phase flow
Qi et al. [72]		•		Inlet quality information missing
Yun et al. [73]	•		•	Horizontal flow boiling in stratified and stratified-wavy flow regime [d]; certain tests performed on circular test section with wire coil inserts
Zhang and Fu [74]		•		Heat flux and local wall temperature information missing
Shirai et al. [18]			•	Data points difficult to extract due to strong overlap
Tatsumoto et al. [19]			•	Only transition boiling data post CHF provided
Fu et al. [75]	•			Boiling from altered surface for enhanced nucleation
Shirai et al. [21]			•	Duplicate data in Shirai et al. [16]
Deng et al. [76]	•			Two-phase flow in heated U-tubes
Mustafi [77]	•			Dry-out occurring in helically shaped pre-heater
Trejo et al. [29]	•			Square and rectangular channel test sections; additional data using roughened and finned square channel test sections
Yoneda et al. [78]	•			Rectangular channel test section with one-sided heating
Fang et al. [79]		•		Only overall range of inlet subcooling provided
Liu et al. [80]		•		Local HTC information provided in the form $h_{min.}/h_{avg.}$
An et al. [81]			•	Film boiling data indistinguishable from transition boiling (*"partial-dryout"*) data; pressure and Inlet quality information missing
Zhang et al. [82]			•	Film boiling data indistinguishable from transition boiling (*"partial-dryout"*) data; only overall range for pressure provided for certain data points and inlet quality information missing for certain data points
(b) Partial Exclusion [b]				
Core et al. [13]			•	Abnormally high scatter reported for LH_2 HTC data owing to experimental uncertainties; transition boiling data post CHF provided
Wright and Walters [14]		•		Only average pressure, mass velocity and quality provided for certain data points; only outer wall temperature provided [e]
Hendricks et al. [83]		•	•	Certain data points presented in tables illegible due to poor quality copy of original document available to public; pressure information missing for certain data points

(*continued on next page*)

Table 2 (*continued*)

Reference	Deviation from standard flow configuration [a]	Missing data	Miscellaneous factors	Remarks
Lewis et al. [15]		•	•	Film boiling data indistinguishable from transition boiling data for certain data points; inlet quality information missing for certain data points; only outer wall temperature provided for both LH_2 and LN_2 data [f]
Hendricks et al. [84]			•	Certain data points presented in tables illegible due to poor quality copy of original document available to public
Glickstein and Whitesides[c] [85]		•		Only overall ranges for pressure and mass velocity provided for certain data points
Papell [86]	•			Certain data points provided for increased gravity loading of 2-g and 3-g
Hynek et al. [48]	•	•		Certain tests performed using twisted tape inserts to generate swirl flow; heat flux and inlet quality information missing for certain data points; certain data points provided for decreasing heat flux
Hildebrandt [1]		•		Only overall range for mass velocity provided for certain data points; certain data points provided for decreasing heat flux
Giarratano et al. [2]		•	•	Film boiling data indistinguishable from transition boiling data for certain data points; heat flux and inlet quality information missing for certain data points
Ogata and Sato [4]		•	•	Certain data points provided for decreasing heat flux; thermocouple position information missing for certain data points
Romanov et al. [7]		•		Heat flux and inlet quality information missing for certain data points
Petukhov et al. [5]	•		•	Certain tests performed on rotating test section; film boiling data indistinguishable from transition boiling data for certain data points
Peroulias et al. [87]		•		Inlet quality information missing for certain data points
Giarratano et al. [61]		•	•	Film boiling data indistinguishable from transition boiling data for certain data points; only overall range of mass velocity and inlet quality provided for certain data points
Tatsumoto et al. [27]			•	Certain data points provided for no-flow condition
Noord [28]			•	Certain data points provided for transient boiling
Xu et al. [88]		•		Inlet quality information missing for certain data points
Matsumoto et al. [24]			•	Certain data points provided for decreasing heat flux
Shirai et al. [89]			•	Certain data points provided for decreasing heat flux

[a] Standard flow configuration is uniformly heated straight circular tube with heat applied externally to single-component fluid.
[b] Select data points are excluded while remaining data are used in the present study.
[c] Pressure and mass velocity information for certain data points provided in Shah [50] and Hynek et al. [48].
[d] Asymmetrical wetting of test section (top-dry and bottom-wet) leads to exorbitantly high wall superheat and drastically low HTC values at the top as compared to the bottom wetted portion.
[e] Inner wall temperature found using one-dimensional radial heat conduction equation with constant outer heat flux boundary condition, q: $T_{w,in} = T_{w,out} - \frac{qD}{2k_w} \ln(\frac{D+2t_w}{D})$.
[f] Inner wall temperature found using one-dimensional radial heat conduction equation with volumetric heat generation, $\dot{q}$: $T_{w,in} = T_{w,out} + \frac{\dot{q}t_w}{4k_w}(D+t_w) - \frac{\dot{q}(D+2t_w)^2}{8k_w} \ln(\frac{D+2t_w}{D})$.

Table 3
Correlation for actual quality, x_a, actual vapor enthalpy, $h_{g,a}$, and actual vapor temperature, $T_{g,a}$, for post-CHF saturated and superheated DFFB for LN_2, using experimentally obtained actual quality information by Forslund and Rohsenow [39].

Correlation	Equation	Constants
75 Data Points MAE (%) = 6.4 RMS (%) = 8.7 θ (%) = 100 ξ (%) = 100 **Fluid:** LN_2 **Flow Direction:** Vertical Upflow **Constraints:** $x_e \geq 0$ $T_{g,a} < T_w$ $T_{g,a} \geq T_{g,e}$	Actual quality, x_a: $x_a = (c_1 + c_2 x_e + c_3 x_e^2 + c_4 x_e^3)\ Fr_{fo}^{c_5}$ if $x_a > x_e$ $x_a = x_e$ if $x_a > 1$ $x_a = 1$ Intersection between $x_a = x_e$ and $x_a = (c_1 + c_2 x_e + c_3 x_e^2 + c_4 x_e^3) Fr_{fo}^{c_5}$ is evaluated by solving them simultaneously to obtain intersection values $x_{a,int}$ and $x_{e,int}$. if $x_a \leq x_{a,int}$ $x_a = x_e$ Actual vapor enthalpy, $h_{g,a}$, and actual vapor temperature, $T_{g,a}$: $h_{g,a} = h_{g,e} + (\frac{x_e - x_a}{x_a}) h_{fg}$ $T_{g,a} = f(P, h_{g,a})$	$c_1 = -0.0179$ $c_2 = 1.0092$ $c_3 = -0.3130$ $c_4 = 0.0325$ $c_5 = 0.0640$

D x 10^3 [m]	P x 10^{-6} [N m^{-2}]	P_R	G [kg m^{-2} s^{-1}]	Fr_{fo}	$T_{g,e}$ [K]	x_e	$T_{g,a}$ [K]	x_a
5.8	0.17	0.05	92.65	0.13	82.00	0.25	82.25	0.21
11.7	0.18	0.05	259.98	1.91	438.37	2.95	450.01	1.00

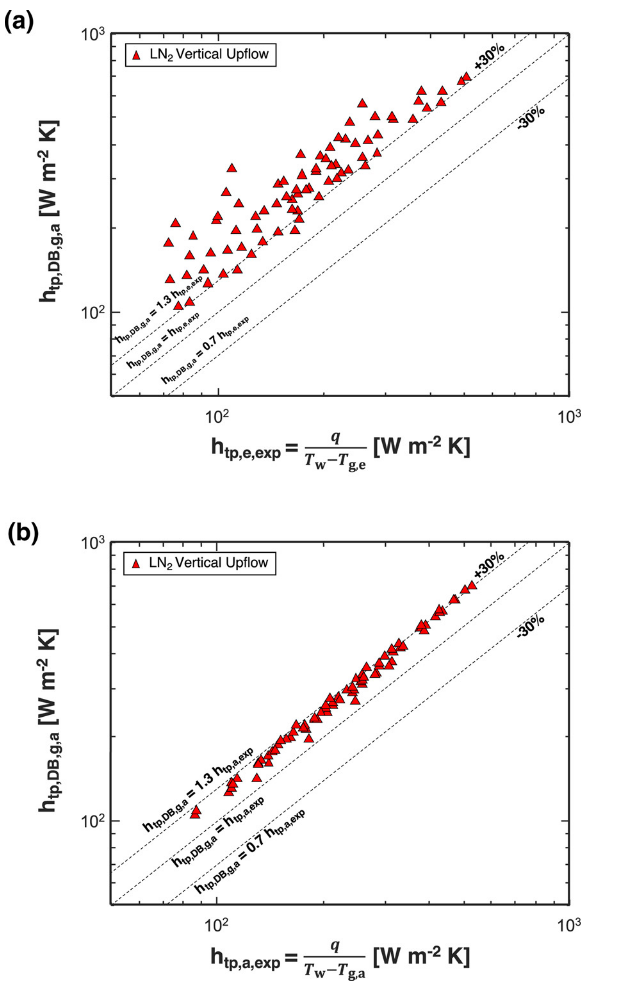

Fig. 9. Comparison of DFFB HTC predicted by modified Dittus-Boelter correlation, Eq. (6), and experimental actual quality, x_a, with experimentally determined two-phase HTC using as reference temperature (a) equilibrium vapor temperature, $T_{g,e}$, and (b) actual vapor temperature, $T_{g,a}$, for LN_2 vertical upflow DFFB data obtained by Forslund and Rohsenow [39].

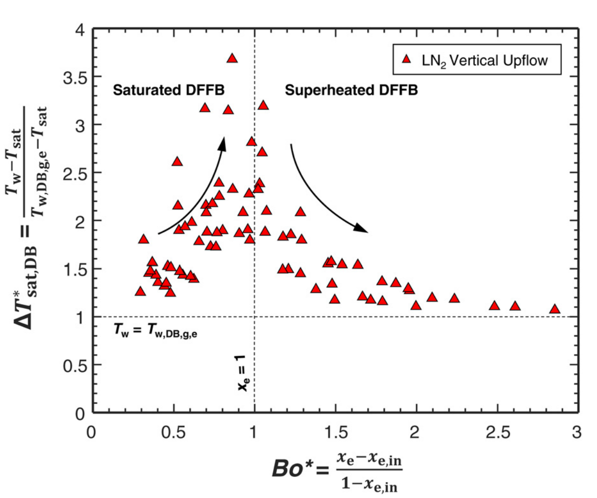

Fig. 10. Demarcating saturated and superheated DFFB flow physics using LN_2 vertical upflow DFFB data by Forslund and Rohsenow [39].

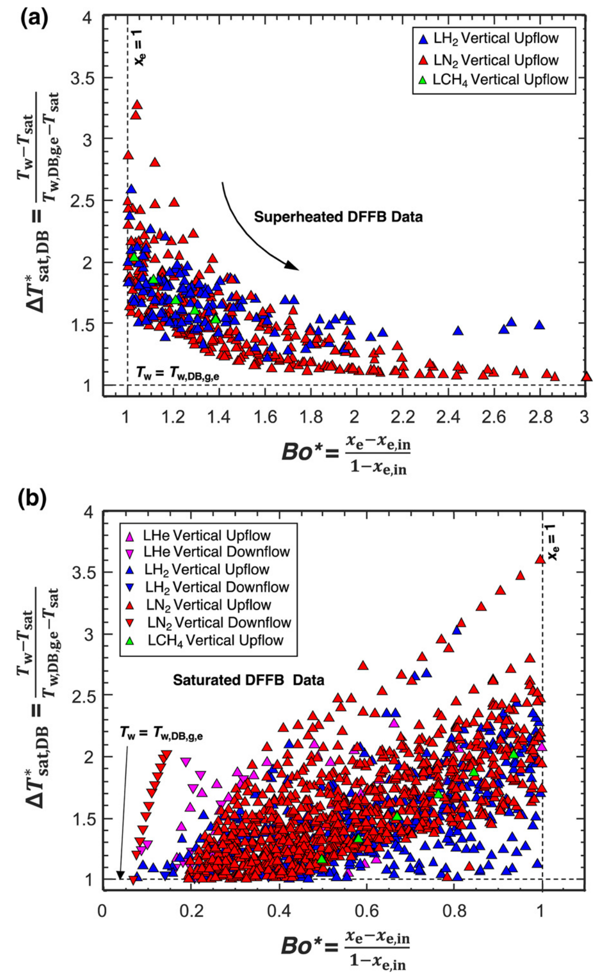

Fig. 11. Trends displayed by (a) superheated and (b) saturated DFFB data from the PU-BTPFL post-CHF Database against proposed classifiers of modified boiling number, Bo^*, and normalized wall temperature, $\Delta T^*_{sat,DB}$.

and based on the Dittus-Boelter [90] formulation using equilibrium quality,

$$\Delta T^*_{sat,DB} = \frac{T_w - T_{sat}}{T_{w,DB,g,e} - T_{sat}}, \tag{8}$$

where

$$T_{w,DB,g,e} = T_{g,e} + \frac{q}{h_{tp,DB,g,e}} = T_{g,e} + \frac{q}{0.023 Re_{g,e}^{0.8} Pr_{g,e}^{0.4} \left(\frac{k_{g,e}}{D}\right)}, \tag{9}$$

and subscript DB refers to Dittus-Boelter formulation. It is clearly seen that there are two distinct trends between the saturated region ($Bo^* \le 1$) and superheated region ($Bo^* > 1$). In the saturated region, $\Delta T^*_{sat,DB}$ increases with increasing Bo^*, whereas, in the superheated region, $\Delta T^*_{sat,DB}$ decreases with increasing Bo^*. However, DFFB data in both regions correspond to $\Delta T^*_{sat,DB} \ge 1$.

3.3. Demarcation of DFFB and IAFB data for Multiple Cryogens

The rationale from Fig. 10 is now tested for all DFFB data in the PU-BTPFL post-CHF HTC Database, which included multiple cryogens rather than LN_2 alone. Fig. 11 clearly confirms the superheated and saturated data display the same trend as that for LN_2 in Fig. 10. Additionally, all the DFFB data obey the criterion $\Delta T^*_{sat,DB} \ge 1$.

We now shift attention to the remaining IAFB data in the PU-BTPFL post-CHF HTC database. Figure 12 shows how almost all of

Table 4
Parameter ranges of acceptable local superheated ($x_e > 1$) dispersed flow film boiling (DFFB) data in the PU-BTPFL post-CHF HTC Database.

Reference	Acceptable HTC data	Tube dimensions		Operating and Inlet Conditions				Local Conditions[a]				HTC Measurements[b]				Remarks
		D x 10^3 [m]	L_H/D	P x 10^{-6} [N m^{-2}]	G [kg m^{-2} s^{-1}]	q x 10^{-3} [W m^{-2}]	$x_{e,in}$	x_e	$T_{g,e}$ [K]	x_a	$T_{g,a}$ [K]	$\Delta T_{w,e}$ [K]	$h_{tp,e}$ [W m^{-2} K^{-1}]	$\Delta T_{w,a}$ [K]	$h_{tp,a}$ [W m^{-2} K^{-1}]	
Liquid Hydrogen																
(a) Vertical Upflow																
Lewis et al. [15]	121	14.1	29.05	0.21	3.87	26.18	−0.13	1	25.57	0.65	40.98	174.6	112.23	153.2	120.46	SS 304 Tube, t_w = 0.89 mm CHF type(s) [c]: DNB DFFB Regime(s) [d]: *post*-IAFB
		14.1	29.05	0.54	18.31	77.6	−0.01	2.86	92.05	0.86	116.16	350.83	313.59	326.72	332.36	
LH_2 HTC data points	**121**															
Liquid Nitrogen																
(a) Vertical Upflow																
Hynek et al. [48]	13	10.16	240	0.14	42.04	22.4	−0.13	1	80.15	0.56	195.99	212.76	51.43	132.19	76.89	Inconel 600 Tube, t_w = 1.27 mm CHF type(s) [c]: Dryout DFFB Regime(s) [d]: *post*-Dryout
		10.16	240	0.14	131.55	38.17	−0.02	2.33	326.94	0.81	432.17	435.51	179.41	291.3	268.95	
Laverty and Rohsenow [46]	48	8.1	149.84	0.12	94.39	33.44	0	1	78.94	0.63	159.16	247.56	110.05	176.71	171.3	SS 304 Tube, t_w = 0.71 mm CHF type(s) [c]: Dryout DFFB Regime(s) [d]: *post*-Dryout
		8.1	149.84	0.14	210.08	83.6	0	1.71	210.82	0.85	272.75	410.49	328.91	303.69	453.44	
Forslund and Rohsenow [*,e] [39]	213	5.79	148.61	0.17	92.65	16.71	−0.06	1	82.95	0.63	146.7	94.93	74.87	56.64	128.92	SS 304 Tube, t_w = 0.51 – 1.07 mm CHF type(s) [c]: DNB DFFB Regime(s) [d]: *post*-IAFB
		11.73	421.05	0.18	263.6	76.71	0	3.06	459.26	1	515.12	449.61	556.75	352.75	659.85	
LN_2 HTC data points	**274**															
Liquid Methane																
(a) Vertical Upflow																
Glickstein and Whitesides [85]	5	8.76	95.65	1.03	207.5	359.53	−0.12	1.03	154.56	0.79	202.38	544.82	547.4	530.08	590.39	Inconel 600 Tube, t_w = 0.38 mm CHF type(s) [c]: DNB DFFB Regime(s) [d]: *post*-IAFB
		8.76	95.65	1.03	207.5	359.53	−0.12	1.43	223.56	0.95	238.29	656.8	659.92	608.98	678.26	
LCH_4 HTC data points	**5**															
Total	**400**															

[*] 6 data points (from Run 290 [39]) rejected due to anomalous wall temperature behavior ($T_w \approx$ constant) with axial location, z, for post-CHF DFFB flow regime.
[a] Actual quality, x_a, evaluated using new universal superheated DFFB HTC correlation in Table 6
$T_{g,a} = f(P, h_{g,a})$, where $h_{g,a}$ is evaluated using Eq. (3).
[b] $h_{tp,e}$ is HTC defined using equilibrium vapor temperature, $T_{g,e}$, as reference temperature, $h_{tp,e} = \frac{q}{T_w - T_{g,e}}$
$h_{tp,a}$ is HTC defined using actual vapor temperature, $T_{g,a}$, as reference temperature, $h_{tp,a} = \frac{q}{T_w - T_{g,a}}$.
[c] CHF type identified using solution strategy adopted in Table 5.
[d] Dispersed Flow Film Boiling (DFFB) regime, dependent on CHF type, is identified from original references.
[e] All data in this reference are associated with non-uniform heat flux conditions due to strong axial conduction, leading to strong axial variations in wall temperature and therefore electrical resistance.

Table 5
Solution strategy to determine CHF location, type (DNB or Dryout) and corresponding equilibrium quality at CHF, $x_{e,CHF}$, for subsequent analysis of post-CHF saturated and superheated flow film boiling data.

For known controlled variables (P, D, G, q) and inlet equilibrium quality ($x_{e,in}$), location of CHF, z_{CHF}, and quality at CHF, $x_{e,CHF}$, are evaluated using universal CHF correlations for cryogens by Ganesan et al. [91]

$\frac{z_{CHF}}{D} = \left(\frac{c_1 We_{fo,D}^{c_2}\left(\frac{\rho_f}{\rho_g}\right)^{c_3}(1-x_{e,in})^{1+c_4}}{4Bo}\right)^{\frac{1}{1-c_5}}$ $x_{e,CHF} = x_{e,in} + 4Bo\frac{z_{CHF}}{D}$ where constants c_1 to c_5 are estimated using the following rationale:

Assuming q corresponds to DNB type CHF, i.e., $\alpha_{CHF} < 0.6$ [91], use constants c_1 to c_5 from table below for specific flow orientation to determine z_{CHF} and $x_{e,CHF}$.

Flow Direction	c_1	c_2	c_3	c_4	c_5
Vertical Flows (*Upflow and Downflow*)	0.19	−0.22	−0.29	1.11	0.57
Horizontal Flow	0.32	−0.24	−0.60	0.48	0.69

If $x_{e,CHF} < 0$
q is confirmed to correspond to DNB-type CHF and z_{CHF} and $x_{e,CHF}$ are estimated correctly. Additionally, check for maximum pressure drop ratio, $\Delta P_{max}/P$, [91] until z_{CHF} of less than 0.2 to make use of the constant pressure assumption.
If $x_{e,CHF} \geq 0$
Evaluate α_{CHF} using Zivi's relation [92]: $\alpha_{CHF} = \left[1 + \left(\frac{1-x_{e,CHF}}{x_{e,CHF}}\right)\left(\frac{\rho_g}{\rho_f}\right)^{2/3}\right]^{-1}$.
if $\alpha_{CHF} < 0.6$ [91]
q is confirmed to correspond to DNB-type CHF and z_{CHF} and $x_{e,CHF}$ are estimated correctly. Additionally check for maximum pressure drop ratio, $\Delta P_{max}/P$, [91] until z_{CHF} of less than 0.2 to make use of the constant pressure assumption.
Otherwise, q corresponds to Dryout-type CHF, i.e., $\alpha_{CHF} \geq 0.6$ [91]. Hence, use constants c_1 to c_5 from table below for specific flow orientations to re-determine z_{CHF} and $x_{e,CHF}$.

Flow Direction	c_1	c_2	c_3	c_4	c_5
Vertical Flows (*Upflow and Downflow*)	0.85	−0.22	−0.22	1.83	0.22
Horizontal Flow	1.1	−0.25	−0.28	−0.60	0.29

Re-evaluate α_{CHF} using Zivi's relation [92]: $\alpha_{CHF} = \left[1 + \left(\frac{1-x_{e,CHF}}{x_{e,CHF}}\right)\left(\frac{\rho_g}{\rho_f}\right)^{2/3}\right]^{-1}$.
if $\alpha_{CHF} \geq 0.6$, q is confirmed to be Dryout-type CHF and z_{CHF} and $x_{e,CHF}$ are estimated correctly. Additionally check for maximum pressure drop ratio, $\Delta P_{max}/P$, [91] until z_{CHF} is less than 0.2 to make use of the constant pressure assumption. Otherwise stop and reject data.

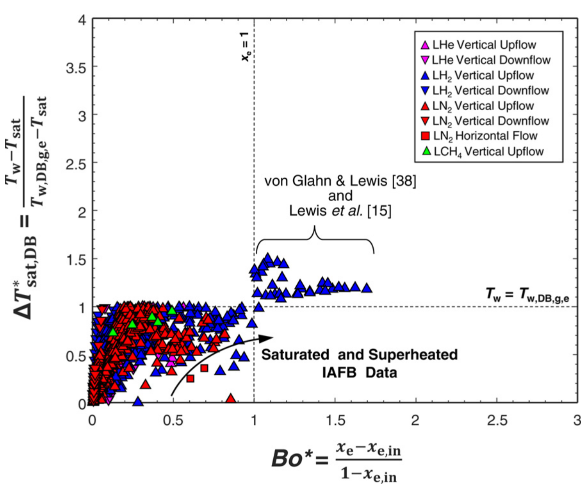

Fig. 12. Trends of local superheated and saturated IAFB data from PU-BTPFL post-CHF HTC Database using classifiers of modified boiling number, Bo^*, and normalized wall temperature, $\Delta T^*_{sat,DB}$.

the IAFB data are in the saturated region ($Bo^* \leq 1$) with a particular set of LH_2 data by von Glahn and Lewis [38] and Lewis et al. [15] incurring superheated IAFB ($Bo^* > 1$). Additionally, it can be observed that for all cryogens undergoing saturated IAFB, $\Delta T^*_{sat,DB} < 1$. Hence, this enables distinction of DFFB data from IAFB data.

3.4. New DFFB Correlations for Multiple Cryogens

Starting with the PU-BTPFL post-CHF HTC database, superheated DFFB data are identified and presented in Table 4. This data subset is used to construct a new universal correlation for superheated DFFB HTC. This requires first determining the CHF type (DNB or Dryout), taking advantage of the cryogenic CHF correlations proposed recently by the authors [91] as detailed in Table 5.

Table 6(a) provides details of the new universal cryogen correlation for superheated ($x_e > 1$) DFFB HTC based on actual quality, x_a, actual vapor enthalpy, $h_{g,a}$, and actual vapor temperature, $T_{g,a}$.

$$h_{tp,a} = 0.8 h_{DB,g,a}, \tag{10a}$$

where $h_{DB,g,a}$ is given by Eq. (6), $Re_{g,a} = GDx_a/\mu_{g,a}$, $Pr_{g,a} = \mu_{g,a}c_{p,g,a}/k_{g,a}$, and all thermophysical properties of vapor evaluated at $T_{g,a}$. It is important to note that the empirical constants associated with estimation of actual quality, x_a, in Table 6(a) are exactly the same as those from Table 3, which was developed using experimentally obtained x_a values for LN_2 DFFB by Forslund and Rohsenow [39].

Table 6(b) provided details of alternative new universal cryogen correlation for superheated ($x_e > 1$) DFFB HTC based on equilibrium quality, x_e, and equilibrium vapor temperature, $T_{g,e}$.

$$h_{tp,e} = 0.5 h_{DB,g,e}(Bo^*)^{0.45}, \tag{10b}$$

where all thermophysical properties of vapor evaluated at $T_{g,e}$. Figure 13 shows comparisons of data with predictions of the two new correlations. Good agreement is achieved in both cases.

Similarly, using now the saturated DFFB data from Table 7 , new universal correlations are developed for saturated ($0 \leq x_e \leq 1$) DFFB HTC. The first, Table 8(a), is based on actual quality, x_a, actual vapor enthalpy, $h_{g,a}$, and actual vapor temperature, $T_{g,a}$, and is given by

$$h_{tp,a} = 0.86 h_{DB,g,a}, \tag{11a}$$

where all thermophysical properties of vapor evaluated at $T_{g,a}$. The second, Table 8(b), is based on based on equilibrium quality, x_e, and equilibrium vapor temperature, $T_{g,e}$, and is given by

$$h_{tp,e} = 0.52 h_{DB,g,e}(Bo^*)^{-0.32}, \tag{11b}$$

where all thermophysical properties of vapor evaluated at $T_{g,e}$. Figure 14 shows excellent predictive accuracy of both correlations.

Table 6
New universal cryogen correlations for superheated ($x_e > 1$) DFFB HTC (a) based on actual quality, x_a, actual vapor enthalpy, $h_{g,a}$, and actual vapor temperature, $T_{g,a}$., and (b) based on equilibrium quality, x_e, and equilibrium vapor temperature, $T_{g,e}$. Both correlations are based on cryogen data from PU-BTPFL post-CHF HTC Database.

Table 6(a)

Correlation	Equation	Constants
400 Data Points MAE (%) = 11.6 RMS (%) = 14.6 θ (%) = 96 ξ (%) = 100 Fluids: LH_2, LN_2, LCH_4 Flow Direction: Vertical Upflow Constraints: Superheated Region ($x_e > 1$) Non-equilibrium Constraints: $T_{g,a} < T_w$ $T_{g,a} \geq T_{g,e}$ DFFB Regime Constraints [a]: $\Delta T^*_{sat,DB} = \frac{T_w - T_{sat}}{T_{w,DB,g,e} - T_{sat}} > 1$	DFFB Heat Transfer Coefficient, $h_{tp,a}$: $h_{tp,a} = \frac{q}{T_w - T_{g,a}} = c_6 h_{DB,g,a}$ where $h_{DB,g,a} = 0.023 Re_{g,a}^{0.8} Pr_{g,a}^{0.4} \frac{k_{g,a}}{D}$ $Re_{g,a} = \frac{G D x_a}{\mu_{g,a}}$ and $Pr_{g,a} = \frac{\mu_{g,a} c_{p,g,a}}{k_{g,a}}$ with all thermophysical properties of vapor evaluated at $T_{g,a}$ Actual quality, x_a: $x_a = (c_1 + c_2 x_e + c_3 x_e^2 + c_4 x_e^3)\ Fr_{fo}^{c_5}$ if $x_a > x_e$ $x_a = x_e$ if $x_a > 1$ $x_a = 1$ Intersection between $x_a = x_e$ and $x_a = (c_1 + c_2 x_e + c_3 x_e^2 + c_4 x_e^3) Fr_{fo}^{c_5}$ is evaluated by solving them simultaneously to obtain intersection values $x_{a,int}$ and $x_{e,int}$. if $x_a \leq x_{a,int}$ $x_a = x_e$ Actual vapor enthalpy, $h_{g,a}$, and actual vapor temperature, $T_{g,a}$: $h_{g,a} = h_{g,e} + \left(\frac{x_e - x_a}{x_a}\right) h_{fg}$ $T_{g,a} = f(h_{g,a}, P)$	$c_1 = -0.0179$ $c_2 = 1.0092$ $c_3 = -0.3130$ $c_4 = 0.0325$ $c_5 = 0.0640$ $c_6 = 0.7956$

$D \times 10^3$ [m]	$P \times 10^{-6}$ [N m^{-2}]	G [kg m^{-2} s^{-1}]	$q \times 10^{-3}$ [W m^{-2}]	Fr_{fo}	x_e	x_a	$T_{g,a}$ [K]	$\Delta T_{w,a}$ [K]	$h_{tp,a}$ [W m^{-2} K^{-1}]
5.79	0.12	3.87	16.71	0.03	1.00	0.57	40.54	58.69	76.17
14.1	1.03	263.60	359.53	3.90	3.06	1.00	482	611.01	673.29

Table 6(b)

Correlation	Equation	Constants
400 Data Points MAE (%) = 12.8 RMS (%) = 17.9 θ (%) = 93 ξ (%) = 97 Fluids: LH_2, LN_2, LCH_4 Flow Direction: Vertical Upflow Constraints: Superheated Region ($x_e > 1$) DFFB Regime Constraints [a]: $\Delta T^*_{sat,DB} = \frac{T_w - T_{sat}}{T_{w,DB,g,e} - T_{sat}} > 1$	DFFB Heat Transfer Coefficient, $h_{tp,e}$: $h_{tp,e} = \frac{q}{T_w - T_{g,e}} = c_1 h_{DB,g,e} (Bo^*)^{c_2}$ where $h_{DB,g,e} = 0.023 Re_{g,e}^{0.8} Pr_{g,e}^{0.4} \frac{k_{g,e}}{D}$ $Re_{g,e} = \frac{GD}{\mu_{g,e}}$ and $Pr_{g,e} = \frac{\mu_{g,e} c_{p,g,e}}{k_{g,e}}$ with all thermophysical properties of vapor are evaluated at $T_{g,e}$ Modified Boiling Number, Bo^*: $Bo^* = \frac{x_e - x_{e,in}}{1 - x_{e,in}} = \frac{4 Bo \frac{z}{D}}{1 - x_{e,in}}$ Equilibrium vapor enthalpy, $h_{g,e}$, and equilibrium vapor temperature, $T_{g,e}$: $h_{g,e} = h_{in} + 4 \frac{q}{G} \frac{z}{D}$ $T_{g,e} = f(h_{g,e}, P)$	$c_1 = 0.4944$ $c_2 = 0.4483$

$D \times 10^3$ [m]	$P \times 10^{-6}$ [N m^{-2}]	G [kg m^{-2} s^{-1}]	$q \times 10^{-3}$ [W m^{-2}]	Bo^*	x_e	x_a	$T_{g,e}$ [K]	$\Delta T_{w,e}$ [K]	$h_{tp,e}$ [W m^{-2} K^{-1}]
5.79	0.12	3.87	16.71	1	1.00	0.56	25.57	94.93	51.43
14.1	1.03	263.60	359.53	3	3.06	1.00	459.26	656.8	659.92

[a] $T_{w,DB,g,e}$ is given by Eq. (9).

It is important to note that the constants associated with estimation of actual quality in Table 8(a) are exactly the same as those from Table 3. Hence, it is systematically proven that the actual quality correlation developed for DFFB in Table 3 is consistent with the DFFB heat transfer coefficient predictions for both saturated and superheated regions.

It is also important to note that both the equilibrium quality-based correlations for superheated DFFB, Table 6(b), and saturated DFFB, Table 8(b), are continuous at $x_e = 1$, since Bo^* is equal to 1 for $x_e = 1$.

Hence, by proving consistency in the estimation of actual quality for DFFB, the following universal correlation is constructed for both saturated and superheated DFFB HTC data, Table 9,

$$h_{tp,a} = 0.86 h_{DB,g,a}, \quad (12)$$

with Fig. 15 demonstrating again excellent predictive accuracy.

3.5. New IAFB Correlation for Multiple Cryogens

Finally, using the saturated and superheated IAFB data, Table 10, the following universal correlation is constructed for IAFB HTC data, Table 11,

$$h_{tp,e} = 0.75 h_{DB,g,e} (Bo^*)^{-0.41}, \quad (13)$$

Fig. 16 shows good predictive accuracy for this correlation.

4. Correlations for MHF and Rewet Temperature

For cryogenic flow boiling with uniformly heated tubes, Minimum Heat Flux (MHF) and Rewet Temperature (RT) data in literature are scarce. Table 12 shows a list of references that have been

Table 7
Parameter ranges of acceptable local saturated ($0 \le x_e \le 1$) dispersed flow film boiling (DFFB) data in the PU-BTPFL post-CHF HTC Database.

Reference	Acceptable HTC data	Tube dimensions		Operating and Inlet Conditions				Local Conditions [a]				HTC Measurements [b]				Remarks
		D x 10^3 [m]	L_H/D	P x 10^{-6} [N m^{-2}]	G [kg m^{-2} s^{-1}]	q x 10^{-3} [W m^{-2}]	$x_{e,in}$	x_e	$T_{g,e}$ [K]	x_a	$T_{g,a}$ [K]	$\Delta T_{w,e}$ [K]	$h_{tp,e}$ [W m^{-2} K^{-1}]	$\Delta T_{w,a}$ [K]	$h_{tp,a}$ [W m^{-2} K^{-1}]	
Liquid Helium																
(a) Vertical Upflow																
Romanov et al. [7]	17	0.47	212.77	0.1	90	0.56	0.22	0.64	4.24	0.64	4.2	0.41	822	0.45	792.59	CHF type [c]: Dryout DFFB Regime [d]: *post*-Dryout
		0.47	212.77	0.1	90	1.49	0.41	0.83	4.24	0.83	4.2	1.47	1460.28	1.51	1355.69	
Ogata and Sato [e] [4]	22	1.09	77.98	0.11	78.77	0.63	−0.06	0.23	4.33	0.23	4.3	0.65	651.73	0.63	666.62	SS Tube, t_w = 0.25 mm CHF type [c]: Dryout DFFB Regime [d]: *post*-Dryout
		1.09	77.98	0.19	92.16	1.42	0.88	1	4.95	0.93	5	2.15	1046.75	2.1	1026.44	
(b) Vertical Downflow																
Giarratano et al. [2]	5	2.13	46.95	0.12	73	1.65	−0.27	0.12	4.42	0.12	4.4	3.07	287.57	3.07	286.82	SS Tube, t_w = 0.16 mm CHF type [c]: DNB DFFB Regime [d]: *post*-IAFB
		2.13	46.95	0.21	153	3.08	−0.04	0.29	5.1	0.29	5.1	8.9	537.62	8.93	536.9	
Giarratano et al. [61]	12	2.13	46.95	0.11	130	1.72	−0.07	0.09	4.33	0.09	4.3	1.47	214.36	1.51	214.02	SS Tube, t_w = 0.16 mm CHF type [c]: DNB DFFB Regime [d]: *post*-IAFB
		2.13	46.95	0.2	630	6.02	0	0.23	5.04	0.23	5	17.03	1168.04	17.05	1136.26	
LHe HTC data points	**56**															
Liquid Hydrogen																
(a) Vertical Upflow																
Lewis et al. [15]	270	14.1	29.05	0.21	4.03	26.18	−0.18	0.17	23.05	0.15	30.6	101.21	120.4	85.36	124.77	SS 304 Tube, t_w = 0.89 mm CHF type [c]: DNB DFFB Regime [d]: *post*-IAFB
		14.1	29.05	0.54	22.59	79.18	0	1	27.64	0.68	49.8	358.95	477.96	346.37	14,309.59	
Hendricks et al. [83]	64	7.95	38.34	0.19	575.65	374.24	−0.12	0.07	22.66	0.07	22.7	119.25	3001.32	119.21	3002.21	Inconel Tube, t_w = 0.78 mm CHF type [c]: DNB DFFB Regime [d]: *post*-IAFB
		7.95	38.34	0.5	1626.45	1650.59	0	0.92	27.23	0.92	27.2	353.23	10,647.23	353.24	10,646.14	
Core et al. [13]	39	4.25	14.93	0.24	376.84	670.04	−0.39	0.13	23.71	0.13	23.7	226.04	2507.9	226.01	2508.26	SS Tube, t_w = 0.25 mm CHF type [c]: DNB DFFB Regime [d]: *post*-IAFB
		4.25	14.93	1.04	1014.53	9838.16	0.03	0.88	31.66	0.88	31.7	687.53	14,309.46	687.52	14,309.59	
Papell [94]	8	12.83	23.76	0.24	194.94	294.16	0	0.27	23.71	0.27	23.7	209.22	1338.77	209.22	1338.74	Inconel X Tube, t_w = 0.25 mm CHF type [c]: DNB DFFB Regime [d]: *post*-IAFB
		12.83	23.76	0.24	194.94	522.96	0	0.56	23.71	0.56	23.7	325.97	1772.54	325.98	1772.51	
Von Glahn and Lewis [f] [38]	1	13.97	29.32	0.34	7.89	61.16	−0.03	0.99	25.28	0.62	46	208.15	293.85	187.42	326.34	SS 347 Tube, t_w = 0.89 mm CHF type [c]: DNB DFFB Regime [d]: *post*-IAFB
		13.97	29.32	0.34	7.89	61.16	−0.03	0.99	25.28	0.62	46	208.15	293.85	187.42	326.34	

(*continued on next page*)

Table 7 (*continued*)

Reference	Acceptable HTC data	Tube dimensions		Operating and Inlet Conditions				Local Conditions [a]				HTC Measurements [b]				Remarks
		D x 10^3 [m]	L_H/D	P x 10^{-6} [N m^{-2}]	G [kg m^{-2} s^{-1}]	q x 10^{-3} [W m^{-2}]	$x_{e,in}$	x_e	$T_{g,e}$ [K]	x_a	$T_{g,a}$ [K]	$\Delta T_{w,e}$ [K]	$h_{tp,e}$ [W m^{-2} K^{-1}]	$\Delta T_{w,a}$ [K]	$h_{tp,a}$ [W m^{-2} K^{-1}]	
(b) Vertical Downflow																
Papell [94]	9	12.83	23.76	0.24	194.94	130.74	0	0.14	23.71	0.14	23.7	160.77	813.23	160.77	813.2	Inconel X Tube, t_w = 0.25 mm CHF type [c]: DNB DFFB Regime [d]: *post*-IAFB
		12.83	23.76	0.24	194.94	522.96	0	0.56	23.71	0.56	23.7	308.46	1811.98	308.47	1811.94	
LH_2 HTC data points	**391**															
Liquid Nitrogen																
(b) Vertical Upflow																
Hynek et al. [48]	7	10.16	240	0.14	42.04	22.4	−0.13	0.4	80.07	0.28	161.8	151.68	52.5	69.95	71.8	Inconel 600 Tube, t_w = 1.27 mm CHF type [c]: Dryout DFFB Regime [d]: *post*-Dryout
		10.16	240	0.14	131.55	38.17	−0.02	1	80.07	0.67	203.3	426.59	251.65	311.96	545.71	
Laverty and Rohsenow [46]	466	8.1	149.84	0.12	94.39	11.74	0	0.19	78.46	0.16	100.8	139.39	61.56	112.64	85.94	SS 304 Tube, t_w = 0.71 mm CHF type [c]: Dryout DFFB Regime [d]: *post*-Dryout
		8.1	149.84	0.14	299.73	92.11	0	1	80.49	0.72	184.3	469.21	385.49	407.93	521.47	
Forslund and Rohsenow [f] [39]	383	5.79	148.61	0.17	92.65	15.39	−0.06	0.15	81.96	0.14	101.7	122.32	64.83	63.14	85.07	SS 304 Tube, t_w = 0.51 – 1.07 mm CHF type(s) [c]: DNB DFFB Regime(s) [d]: *post*-IAFB
		11.73	421.05	0.18	263.6	78.66	0	1	82.84	0.75	191	530.17	313.2	471.32	481.15	
Lewis et al. [15]	9	14.1	29.05	0.34	33.09	33.28	−0.01	0.46	89.46	0.3	180.6	559.83	51.46	467.49	58.37	SS 304 Tube, t_w = 0.89 mm CHF type(s) [c]: DNB, Dryout DFFB Regime(s) [d]: *post*-IAFB, *post*-Dryout
		14.1	29.05	0.35	37.97	46.37	−0.01	0.86	89.78	0.5	216.7	901.09	59.45	794.47	71.19	
(b) Vertical Downflow																
Umekawa et al. [93]	12	5	180	0.1	138	9.5	−0.01	0.06	77.35	0.05	120.8	235.77	35.75	147.22	44.62	SS 304 Tube, t_w = 0.5 mm CHF type(s) [c]: Dryout DFFB Regime(s) [d]: *post*-Dryout
		5	180	0.1	138	9.5	−0.01	0.14	77.35	0.12	165.9	265.74	40.29	212.89	64.53	
LN_2 HTC data points	**877**															
Liquid Methane																
(a) Vertical Upflow																
Glickstein and Whitesides [85]	6	8.76	95.65	1.03	207.5	359.53	−0.12	0.44	149.88	0.41	164.2	664.48	514.21	621.76	524.96	Inconel 600 Tube, t_w = 0.38 mm CHF type [c]: DNB DFFB Regime [d]: *post*-IAFB
		8.76	95.65	1.03	207.5	359.53	−0.12	0.93	149.88	0.75	192.6	699.2	541.07	684.88	578.25	
LCH_4 HTC data points	**6**															
Total	**1330**															

[a] Actual quality, x_a, evaluated using new universal superheated DFFB HTC correlation in Table 8
$T_{g,a} = f(P, h_{g,a})$, where $h_{g,a}$ is evaluated using Eq. (3).

[b] $h_{tp,e}$ is HTC defined using equilibrium vapor temperature, $T_{g,e}$, as reference temperature, $h_{tp,e} = \frac{q}{T_w - T_{g,e}}$
$h_{tp,a}$ is HTC defined using actual vapor temperature, $T_{g,a}$, as reference temperature, $h_{tp,a} = \frac{q}{T_w - T_{g,a}}$.

[c] CHF type identified using solution strategy adopted in Table 5.

[d] Dispersed Flow Film Boiling (DFFB) regime, dependent on CHF type, is identified from original references.

[e] 1 data point corresponds to DNB type CHF and thus *post*-IAFB type DFFB regime.

[f] All data in this reference are associated with non-uniform heat flux conditions due to strong axial conduction, leading to strong axial variations in wall temperature and therefore electrical resistance.

Table 8
New universal cryogen correlations for saturated ($0 \le x_e \le 1$) DFFB HTC (a) based on actual quality, x_a, actual vapor enthalpy, $h_{g,a}$, and actual vapor temperature, $T_{g,a}$, and (b) based on equilibrium quality, x_e, and equilibrium vapor temperature, $T_{g,e}$. Both correlations are based on cryogen data from PU-BTPFL post-CHF HTC Database.

Table 8(a)

Correlation	Equation	Constants
1330 Data Points MAE (%) = 16.8 RMS (%) = 20.7 θ (%) = 86 ξ (%) = 99 **Fluids:** LHe, LH_2, LN_2, LCH_4 **Flow Direction:** Vertical Upflow Vertical Downflow **Constraints:** Saturated Region ($0 \le x_e \le 1$) Non-equilibrium Constraints: $T_{g,a} < T_w$ $T_{g,a} \ge T_{g,e}$ DFFB Regime Constraints [a]: $\Delta T^*_{sat,DB} = \frac{T_w - T_{sat}}{T_{w,DB,g,e} - T_{sat}} > 1$ (±10%)	DFFB Heat Transfer Coefficient, $h_{tp,a}$: $h_{tp,a} = \frac{q}{T_w - T_{g,a}} = c_6 h_{DB,g,a}$ where $h_{DB,g,a} = 0.023 Re_{g,a}^{0.8} Pr_{g,a}^{0.4} \frac{k_{g,a}}{D}$ $Re_{g,a} = \frac{G D x_a}{\mu_{g,a}}$ and $Pr_{g,a} = \frac{\mu_{g,a} c_{p,g,a}}{k_{g,a}}$ with all thermophysical properties of vapor are evaluated at $T_{g,a}$ Actual quality, x_a: $x_a = (c_1 + c_2 x_e + c_3 x_e^2 + c_4 x_e^3) Fr_{fo}^{c_5}$ if $x_a > x_e$ $x_a = x_e$ if $x_a > 1$ $x_a = 1$ Intersection between the curves: $x_a = x_e$, and $x_a = (c_1 + c_2 x_e + c_3 x_e^2 + c_4 x_e^3) Fr_{fo}^{c_5}$ is evaluated by solving them simultaneously to get $x_{a,int}$ and $x_{e,int}$. if $x_a \le x_{a,int}$ $x_a = x_e$ Actual vapor enthalpy, $h_{g,a}$, and actual vapor temperature, $T_{g,a}$: $h_{g,a} = h_g + \left(\frac{x_e - x_a}{x_a}\right) h_{fg}$ $T_{g,a} = f(h_{g,a}, P)$	$c_1 = -0.0179$ $c_2 = 1.0092$ $c_3 = -0.3130$ $c_4 = 0.0325$ $c_5 = 0.0640$ $c_6 = 0.8565$

$D \times 10^3$ [m]	$P \times 10^{-6}$ [N m^{-2}]	G [kg m^{-2} s^{-1}]	$q \times 10^{-3}$ [W m^{-2}]	Fr_{fo}	x_e	x_a	$T_{g,a}$ [K]	$\Delta T_{w,a}$ [K]	$h_{tp,a}$ [W m^{-2} K^{-1}]
0.47	0.10	4.03	0.56	0.01	0.06	0.04	4.24	0.41	44.63
14.1	1.04	1626.5	9838.2	8902.9	1.00	0.92	216.74	794.44	14,309

Table 8(b)

Correlation	Equation	Constants
1330 Data Points MAE (%) = 16.1 RMS (%) = 20.9 θ (%) = 90 ξ (%) = 97 **Fluids:** LHe, LH_2, LN_2, LCH_4 **Flow Direction:** Vertical Upflow Vertical Downflow **Constraints:** Superheated Region ($x_e > 1$) DFFB Regime Constraints [a]: $\Delta T^*_{sat,DB} = \frac{T_w - T_{sat}}{T_{w,DB,g,e} - T_{sat}} > 1$ (±10%)	DFFB Heat Transfer Coefficient, $h_{tp,e}$: $h_{tp,e} = \frac{q}{T_w - T_{v,e}} = c_1 h_{DB,g,e} (Bo^*)^{c_2}$ where $h_{DB,g,e} = 0.023 Re_{g,e}^{0.8} Pr_{g,e}^{0.4} \frac{k_{g,e}}{D}$ $Re_{g,e} = \frac{G D}{\mu_{g,e}}$ and $Pr_{g,e} = \frac{\mu_{g,e} c_{p,g,e}}{k_{g,e}}$ with all thermophysical properties of vapor are evaluated at $T_{g,e}$ Modified Boiling Number, Bo^*: $Bo^* = \frac{x_e - x_{e,in}}{1 - x_{e,in}} = \frac{4 Bo \frac{z}{D}}{1 - x_{e,in}}$ Equilibrium vapor enthalpy, $h_{g,e}$, and equilibrium vapor temperature, $T_{g,e}$: $h_{g,e} = h_{in} + 4 \frac{q}{G} \frac{z}{D}$ $T_{g,e} = f(h_{g,e}, P)$	$c_1 = 0.5236$ $c_2 = -0.3243$

$D \times 10^3$ [m]	$P \times 10^{-6}$ [N m^{-2}]	G [kg m^{-2} s^{-1}]	$q \times 10^{-3}$ [W m^{-2}]	Bo^*	x_e	x_a	$T_{g,e}$ [K]	$\Delta T_{w,e}$ [K]	$h_{tp,e}$ [W m^{-2} K^{-1}]
0.47	0.10	4.03	0.56	0.07	0.06	0.04	4.24	0.41	35.75
14.1	1.04	1626.5	9838.2	1.00	1.00	0.92	149.88	901.09	14,309

[a] $T_{w,DB,g,e}$ is given by Eq. (9).

Table 9
New universal cryogen correlation for saturated and superheated DFFB HTC based on actual quality, x_a, actual vapor enthalpy, $h_{g,a}$, and actual vapor temperature, $T_{g,a}$. This correlation is based on cryogen data from PU-BTPFL post-CHF HTC Database.

Correlation	Equation	Constants
1730 Data Points MAE (%) = 16.0 RMS (%) = 20.0 θ (%) = 87 ξ (%) = 98 Fluids: LHe, LH_2, LN_2, LCH_4 Flow Direction: Vertical Upflow Vertical Downflow Constraints: $x_e > 0$ Non-equilibrium Constraints: $T_{v,a} < T_w$ $T_{v,a} \geq T_{v,e}$ DFFB Regime Constraints [a]: $\Delta T^*_{sat,DB} = \frac{T_w - T_{sat}}{T_{w,DB,g,e} - T_{sat}} > 1$ (−10%)	DFFB Heat Transfer Coefficient, $h_{tp,a}$: $h_{tp,a} = \frac{q}{T_w - T_{g,a}} = c_6 h_{DB,g,a}$ where $h_{DB,v,a} = 0.023 Re_{g,a}^{0.8} Pr_{v,a}^{0.4} \frac{k_{v,a}}{D}$ $Re_{g,a} = \frac{G D x_a}{\mu_{g,a}}$ and $Pr_{g,a} = \frac{\mu_{g,a} c_{p,g,a}}{k_{g,a}}$ with all thermophysical properties of vapor evaluated at $T_{g,a}$ Actual quality, x_a: $x_a = (c_1 + c_2 x_e + c_3 x_e^2 + c_4 x_e^3)\ Fr_{fo}^{c_5}$ if $x_a > x_e$ $x_a = x_e$ if $x_a > 1$ $x_a = 1$ Intersection between $x_a = x_e$ and $x_a = (c_1 + c_2 x_e + c_3 x_e^2 + c_4 x_e^3) Fr_{fo}^{c_5}$ is evaluated by solving them simultaneously to obtain intersection values $x_{a,int}$ and $x_{e,int}$. if $x_a \leq x_{a,int}$ $x_a = x_e$ Actual vapor enthalpy, $h_{g,a}$, and actual vapor temperature, $T_{g,a}$: $h_{g,a} = h_{g,e} + \left(\frac{x_e - x_a}{x_a}\right) h_{fg}$ $T_{g,a} = f(h_{g,a}, P)$	$c_1 = -0.0179$ $c_2 = 1.0092$ $c_3 = -0.3130$ $c_4 = 0.0325$ $c_5 = 0.0640$ $c_6 = 0.8608$

$D \times 10^3$ [m]	$P \times 10^{-6}$ [N m^{-2}]	G [kg m^{-2} s^{-1}]	$q \times 10^{-3}$ [W m^{-2}]	Fr_{fo}	x_e	x_a	$T_{g,a}$ [K]	$\Delta T_{w,a}$ [K]	$h_{tp,a}$ [W m^{-2} K^{-1}]
0.47	0.10	3.87	0.56	0.01	0.06	0.04	4.24	0.41	44.63
14.1	1.04	1626.5	9838.2	8902.9	3.06	1.00	482	794.44	14,309

[a] $T_{w,DB,g,e}$ is given by Eq. (9).

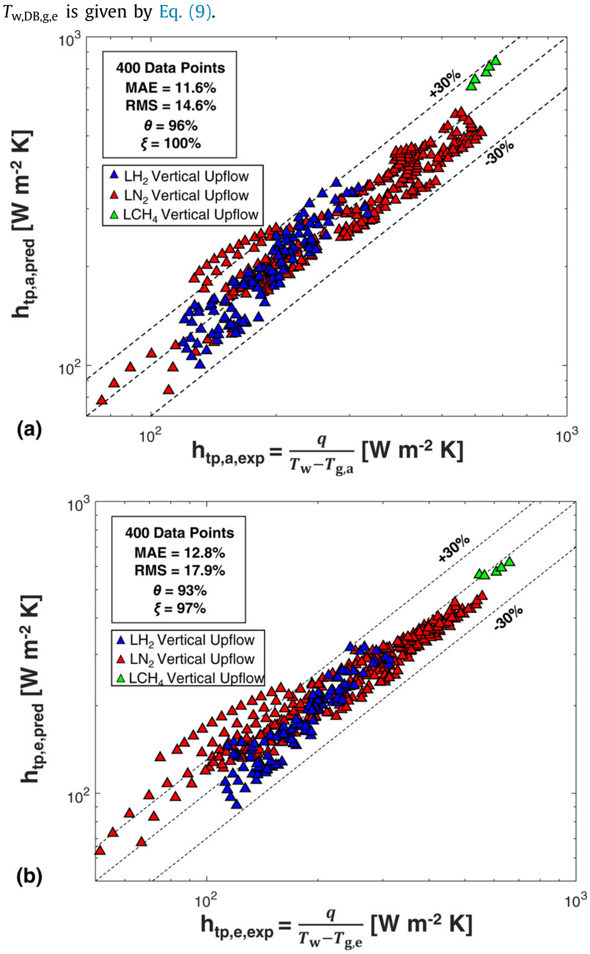

Fig. 13. Comparison of cryogen data from PU-BTPFL post-CHF HTC Database with predictions of new universal correlations for superheated ($x_e > 1$) DFFB HTC (a) based on actual (non-equilibrium) quality, x_a, actual (non-equilibrium) vapor enthalpy, $h_{g,a}$, and actual (non-equilibrium) vapor temperature, $T_{g,a}$, and (b) based on equilibrium quality, x_e, and equilibrium vapor temperature, $T_{g,e}$.

excluded for consideration. The final acceptable local MHF and local RT databases are provided in Table 13.

The functional form for MHF is chosen to be the same as that of CHF which was proposed by the present authors in Ganesan et al. [91]. However, this requires knowledge of z_{MHF}, axial location of MHF. Since not all data in the MHF database include information on z_{MHF}, a hypothesis is proposed and later verified that approximates the position of MHF as the last location of z_{CHF} corresponding to q_{max}. This hypothesis is explained in Fig. 17 for uniformly heated tubes undergoing IAFB as the flow regime transitions from film to nucleate boiling via the re-wetting process. At $q = q_{DNB}$, DNB type CHF is observed at $z_{CHF} = z_{DNB}$, as shown in Fig. 17(a). With further heat increments post q_{DNB} toward q_{max}, CHF location moves upstream as more and more vapor bubbles coalesce and merge into the existing vapor film. At $q = q_{max}$, which corresponds to the maximum heat flux provided to the test section before heat decrement, the inverted annular film extends from z_{DNB} onward until the liquid jet core breaks down and gets dispersed into the vapor continuum. This is shown in Fig. 17(b). From here on, as the heat flux is reduced toward q_{MHF}, z_{DNB} can neither move upstream (due to heat decrement) nor downstream (due to stable film boiling prevalent downstream of z_{DNB}). Hence z_{DNB} is anchored at z_{CHF} corresponding to q_{max}, as shown in Fig. 17(c). At q_{MHF}, since the vapor film is the thinnest at z_{DNB}, this is where the film is more likely to become unstable and collapse, leading to rewetting of the surface. Hence, the location of MHF becomes the same as the location of DNB at q_{max}. This is shown in Fig. 17(d). As the heat flux is further decreased from q_{MHF}, since the vapor film is no longer stable, z_{MHF} starts to propagate downstream, as shown in Fig. 17(e). Employing this hypothesis, a new universal correlation for MHF is proposed in Table 14,

$$q_{MHF} = 0.07 G h_{fg} We_{fo,D}^{-0.34} \left(\frac{\rho_f}{\rho_g}\right)^{-0.54} (1 - x_{e,in})^{0.65} \left(\frac{z_{MHF}}{D}\right)^{-0.44}, \quad (14)$$

Table 10
Parameter ranges of acceptable local saturated ($0 \leq x_e \leq 1$) and superheated* ($x_e > 1$) inverted annular film boiling (IAFB) data in the PU-BTPFL post-CHF HTC Database.

Reference	Acceptable HTC data	Tube dimensions		Operating and Inlet Conditions				Local Conditions		HTC Measurements [a]		Remarks
		D x 10^3 [m]	L_H/D	P x 10^{-6} [N m^{-2}]	G [kg m^{-2} s^{-1}]	q x 10^{-3} [W m^{-2}]	$x_{e,in}$	x_e	$T_{g,e}$ [K]	$\Delta T_{w,e}$ [K]	$h_{tp,e}$ [W m^{-2} K^{-1}]	
Liquid Helium												
(a) Vertical Upflow												
Romanov et al. [7]	11	0.47	212.77	0.1	90	0.45	0.22	0.59	4.24	0.18	1463.22	CHF type [c] : DNB IAFB Regime [d]: *post*-DNB
		0.47	212.77	0.1	90	1.15	0.41	0.66	4.24	0.7	3391.15	
Yarmak and Zhukov [97]	7	0.8	187.5	0.1	78	1.54	0	0.24	4.22	1.98	654.15	SS Tube, t_w = 0.1 mm CHF type [c] : DNB IAFB Regime [d]: *post*-DNB
		0.8	187.5	0.1	235	5.93	0	0.44	4.22	2.99	2531.96	
Ogata and Sato [4]	5	1.09	77.98	0.11	82.52	0.63	0.31	0.46	4.33	0.45	1147.58	SS Tube, t_w = 0.25 mm CHF type [c] : DNB IAFB Regime [d]: *post*-DNB
		1.09	77.98	0.11	92.16	1.42	0.51	0.59	4.33	1.16	1825.27	
(b) Vertical Downflow												
Giarratano et al. [2]	8	2.13	46.95	0.14	80	1.6	−0.38	0.03	4.55	2	570.38	SS Tube, t_w = 0.16 mm CHF type [c] : DNB IAFB Regime [d]: *post*-DNB
		2.13	46.95	0.21	636	5.3	−0.01	0.12	5.1	3.92	2656.05	
Giarratano et al. [61]	43	2.13	46.95	0.11	45	1.63	−0.3	0	4.33	0.67	406.61	SS Tube, t_w = 0.16 mm CHF type [c] : DNB IAFB Regime [d]: *post*-DNB
		2.13	46.95	0.2	630	10.13	0	0.39	5.04	8.26	4207.78	
LHe HTC data points	**74**											
Liquid Hydrogen												
(a) Vertical Upflow												
Lewis et al. [15]	201	14.1	29.05	0.21	3.87	19.72	−0.18	0.01	23.05	28.65	141.96	SS 304 Tube, t_w = 0.89 mm CHF type [c] : DNB IAFB Regime [d]: *post*-DNB
		14.1	29.05	0.54	23	79.18	0	1.54	43.22	433.78	740.38	
von Glahn and Lewis [b] [38]	17	13.97	29.32	0.34	7.89	48.05	−0.03	0.54	25.28	99.08	239.72	SS 347 Tube, t_w = 0.89 mm CHF type [c] : DNB IAFB Regime [d]: *post*-DNB
		13.97	29.32	0.34	7.89	65.97	−0.03	1.71	49.67	272.81	484.99	
Papell [94]	25	12.83	23.76	0.24	194.94	130.74	0	0.02	23.71	137.42	894.42	Inconel X Tube, t_w = 0.25 mm CHF type [c] : DNB IAFB Regime [d]: *post*-DNB
		12.83	23.76	0.24	194.94	522.96	0	0.32	23.71	425.8	1819.34	
Core et al. [13]	47	4.25	14.93	0.21	376.84	621.01	−0.39	0	23.19	201.06	2905.63	SS Tube, t_w = 0.25 mm CHF type [c] : DNB IAFB Regime [d]: *post*-DNB
		4.25	14.93	1.03	1014.53	5589.12	0	0.77	31.61	526.04	11,658.16	
Hendricks et al. [83]	118	7.95	38.34	0.19	575.65	374.24	−0.12	0	22.66	72.13	2931.41	Inconel Tube, t_w = 0.78 mm CHF type [c] : DNB IAFB Regime [d]: *post*-DNB
		7.95	38.34	0.5	1653.86	1650.59	0	0.71	27.23	386.95	17,359.39	

(*continued on next page*)

Table 10 (*continued*)

Reference	Acceptable HTC data	Tube dimensions		Operating and Inlet Conditions				Local Conditions		HTC Measurements [a]		Remarks
		D x 10^3 [m]	L_H/D	P x 10^{-6} [N m^{-2}]	G [kg m^{-2} s^{-1}]	q x 10^{-3} [W m^{-2}]	$x_{e,in}$	x_e	$T_{g,e}$ [K]	$\Delta T_{w,e}$ [K]	$h_{tp,e}$ [W m^{-2} K^{-1}]	
(b) Vertical Downflow												
Papell [94]	39	12.83	23.76	0.24	194.94	32.68	0	0	23.71	100.05	300.38	Inconel X Tube, t_w = 0.25 mm CHF type [c] : DNB IAFB Regime [d]: *post*-DNB
		12.83	23.76	0.24	194.94	522.96	0	0.32	23.71	552.48	1823.04	
(c) Horizontal Flow												
Wright and Walters [14]	66	6.35	24	0.15	412.57	66.2	0.01	0.02	21.8	20.47	2263.89	Copper Tube, t_w = 6.35 mm CHF type [c] : DNB IAFB Regime [d]: *post*-DNB
		6.35	24	0.25	956.96	390	0.02	0.21	23.9	167.25	6058.64	
LH_2 HTC data points	**513**											
Liquid Nitrogen												
(a) Vertical Upflow												
Hynek et al. [48]	3	10.16	240	0.14	42.04	22.4	−0.13	0.13	80.07	99.88	68.91	Inconel 600 Tube, t_w = 1.27 mm CHF type [c] : DNB IAFB Regime [d]: *post*-DNB
		10.16	240	0.14	131.55	38.17	−0.02	0.81	80.07	325.02	382.16	
Laverty and Rohsenow [46]	416	8.1	149.84	0.12	94.39	11.74	0	0.01	78.46	100.51	68.11	SS 304 Tube, t_w = 0.71 mm CHF type [c] : DNB IAFB Regime [d]: *post*-DNB
		8.1	149.84	0.14	299.73	92.11	0	0.43	80.49	541.43	339.51	
Forslund and Rohsenow [b] [39]	143	5.79	148.61	0.17	92.65	14.8	−0.06	0	81.96	135.01	75.91	SS 304 Tube, t_w = 0.51 – 1.07 mm CHF type [c] : DNB IAFB Regime [d]: *post*-DNB
		11.73	421.05	0.18	263.6	94.16	0	0.3	82.84	637.89	298.5	
Xu et al. [88]	1	14	71.43	1.07	54.12	24.2	0	0.85	104.8	4.41	5483.44	SS 304 Tube, t_w = 1 mm CHF type [c] : DNB IAFB Regime [d]: *post*-DNB
		14	71.43	1.07	54.12	24.2	0	0.85	104.8	4.41	5483.44	
Lewis et al. [15]	52	14.1	29.05	0.33	23.1	27.98	−0.04	0.13	89.13	123.87	58.7	SS 304 Tube, t_w = 0.89 mm CHF type [c] : DNB IAFB Regime [d]: *post*-DNB
		14.1	29.05	0.39	57.37	46.37	−0.01	0.76	90.81	789.93	268.69	
Papell [96]	81	12.83	23.76	0.24	516.45	11.45	−0.01	0	85.55	62.39	127.71	Inconel X Tube, t_w = 0.25 mm CHF type c : DNB IAFB Regime d: post-DNB
		12.83	23.76	0.24	1760.63	85.38	−0.01	0.05	85.55	527.67	225.11	

(*continued on next page*)

Table 10 (*continued*)

Reference	Acceptable HTC data	Tube dimensions		Operating and Inlet Conditions				Local Conditions		HTC Measurements [a]		Remarks
		D x 10^3 [m]	L_H/D	P x 10^{-6} [N m^{-2}]	G [kg m^{-2} s^{-1}]	q x 10^{-3} [W m^{-2}]	$x_{e,in}$	x_e	$T_{g,e}$ [K]	$\Delta T_{w,e}$ [K]	$h_{tp,e}$ [W m^{-2} K^{-1}]	
(b) Vertical Downflow												
Papell [96]	14	12.83	23.76	0.24	399.08	8.44	−0.01	0	85.55	292.44	24.09	Inconel X Tube, t_w = 0.25 mm CHF type c : DNB IAFB Regime d: post-DNB
		12.83	23.76	0.24	1760.63	94.96	−0.01	0.01	85.55	477.22	214.39	
Umekawa et al. [93]	6	5	180	0.1	138	9.5	−0.01	0.02	77.35	195.85	37.28	SS 304 Tube, t_w = 0.5 mm CHF type [c] : DNB IAFB Regime [d]: *post*-DNB
		5	180	0.1	138	9.5	−0.01	0.06	77.35	254.84	48.51	
(c) Horizontal Flow												
Zhang et al. [95]	2	2.92	204.97	0.33	235	43.6	0	0.61	88.98	23.36	1450.14	SS Tube, t_w = 1 mm CHF type [c] : DNB IAFB Regime [d]: *post*-DNB
		2.92	204.97	0.33	235	43.6	0	0.69	88.98	30.07	1866.33	
LN_2 HTC data points	**718**											
Liquid Methane												
(a)Vertical Upflow												
Glickstein and Whitesides [85]	5	8.76	95.65	1.03	92.22	214.51	−0.12	0.33	149.88	407.57	502.9	Inconel 600 Tube, t_w = 0.38 mm CHF type [c] : DNB IAFB Regime [d]: *post*-DNB
		8.76	95.65	1.03	207.5	359.53	0.5	0.75	149.88	628.81	571.77	
LCH_4 HTC data points	**5**											
Total	**1310**											

[*] Superheated IAFB data are available only for LH_2 by von Glahn and Lewis [38] and Lewis et al. [15].
[a] $h_{tp,e}$ is HTC defined using equilibrium vapor temperature, $T_{g,e}$, as reference temperature, $h_{tp,e} = \frac{q}{T_w - T_{g,e}}$.
[b] All data in this reference are associated with non-uniform heat flux conditions due to strong axial conduction, leading to strong axial variations in wall temperature and therefore electrical resistance.
[c] CHF type identified using solution strategy adopted in Table 5.
[d] Inverted Annular Film Boiling (IAFB) regime, dependent on CHF type, is identified from original references.

Table 11
New universal cryogen correlation for saturated and superheated* IAFB HTC based on equilibrium quality, x_e, and equilibrium vapor temperature, $T_{g,e}$. This correlation is based on cryogen data from PU-BTPFL post-CHF HTC Database.

Correlation	Equation	Constants
1310 Data Points MAE (%) = 26.8 RMS (%) = 35.2 θ (%) = 65 ξ (%) = 86 **Fluids:** LHe, LH_2, LN_2, LCH_4 **Flow Direction:** Vertical Upflow Vertical Downflow Horizontal Flow **Constraints:** $x_e > 0$ IAFB Regime Constraints [a]: $\Delta T^*_{sat,DB} = \frac{T_w - T_{sat}}{T_{w,DB,g,e} - T_{sat}} \le 1$ (+10%)	DFFB Heat Transfer Coefficient, $h_{tp,e}$: $h_{tp,e} = \frac{q}{T_w - T_{g,e}} = c_1 h_{DB,g,e} (Bo^*)^{c_2}$ where $h_{DB,g,e} = 0.023 Re_{g,e}^{0.8} Pr_{g,e}^{0.4} \frac{k_{v,e}}{D}$ $Re_{g,e} = \frac{GD}{\mu_{g,e}}$ and $Pr_{g,e} = \frac{\mu_{g,e} c_{p,g,e}}{k_{g,e}}$ with all thermophysical properties of vapor are evaluated at $T_{g,e}$ Modified Boiling Number, Bo^*: $Bo^* = \frac{x_e - x_{e,in}}{1 - x_{e,in}} = \frac{4Bo \frac{z}{D}}{1 - x_{e,in}}$ Equilibrium vapor enthalpy, $h_{g,e}$, and equilibrium vapor temperature, $T_{g,e}$: $h_{g,e} = h_{in} + 4 \frac{q}{G} \frac{z}{D}$ $T_{g,e} = f(h_{g,e}, P)$	$c_1 = 0.7484$ $c_2 = -0.4133$

D x 10^3 [m]	P x 10^{-6} [N m^{-2}]	G [kg m^{-2} s^{-1}]	q x 10^{-3} [W m^{-2}]	Bo^*	x_e	$T_{g,e}$ [K]	$\Delta T_{w,e}$ [K]	$h_{tp,e}$ [W m^{-2} K^{-1}]
0.47	0.10	3.87	0.45	0	0	4.22	0.18	24.09
14.1	1.07	1760.6	5589.1	1.7	1.71	149.88	789.93	17,359

* Superheated IAFB data are available only for LH_2 by von Glahn and Lewis [38] and Lewis et al. [15].
[a] $T_{w,DB,g,e}$ is given by Eq. (9).

Table 12
Data exclusion strategy for local minimum heat flux (MHF) and re-wet wall temperature (RT) data for sub-critical cryogenic flow boiling in uniformly heated straight circular tubes.

Reference	Deviation from standard flow configuration [a]	Missing data	Miscellaneous factors	Remarks
(a) Complete Exclusion				
von Glahn and Lewis [38]		•		Only overall range for pressure provided for certain data points, and inlet quality information missing
Laverty and Rohsenow [46]		•		Only values of minimum heat flux and mass velocity provided [c]
Forslund and Rohsenow [39]		•		Only values of minimum heat flux, mass velocity, and tube diameter provided
Hynek et al. [48]	•	•		Certain tests performed using twisted tape inserts to generate swirl flow; inlet quality information missing
Jergel & Stevenson [56]	•			Free convection laminar flow in rectangular channel test section with only a small fraction of test section heated
Noord [28]			•	Only transient boiling data provided for decreasing heat flux
Matsumoto et al. [24]		•	•	Heat flux information missing for certain data points; uncertainty in extraction of q_{MHF} and $T_{w,rewet}$ information from boiling (average) curves [d]
Shirai et al. [89]		•	•	Certain data points unclear due to lots of scatter; heat flux information missing for certain data points; uncertainty in extraction of q_{MHF} and $T_{w,rewet}$ information from boiling (average) curves [d]; certain data points display anomalous transition [e] from film to nucleate boiling at MHF
(b) Partial Exclusion [b]				
Hildebrandt [1]		•		Only overall range for mass velocity provided for certain data points
Ogata and Sato [4]	•	•		Certain data points display anomalous transition [e] from film to nucleate boiling at MHF; only overall range for pressure and mass velocity provided for certain data points
Panek et al. [69]	•	•		Certain tests performed under no-flow conditions; q_{max} (maximum heat flux post-CHF attained before decreasing the heat input as seen in Figure 17) information missing for certain data points to estimate z_{MHF}

[a] Standard flow configuration is uniformly heated straight circular tube with deceasing heat input applied externally to single-component fluid.
[b] Select data points are excluded while remaining data are used in the present study.
[c] Reported in Forslund and Rohsenow [39].
[d] For average boiling curves (q versus $\Delta \bar{T}_{w,e}$), obtained by decreasing the heat flux, average wall temperature is heated-length weighted arithmetic average of wall temperatures from two distinct heat transfer regimes: nucleate boiling (*pre*-MHF) and film boiling (*post*-MHF). Hence, despite MHF occurring, if the heated length corresponding to the nucleate boiling (*pre*-MHF) is smaller than that of the film boiling (*post*-MHF), the average wall temperature might not accurately show the transition, therefore creating uncertainty in estimating q_{MHF} and $T_{w,rewet}$ from boiling (average) curves.
[e] For local boiling curves (q versus $\Delta T_{w,e}$) generating by decreasing the heat flux, there is an abrupt jump at MHF when transitioning from film to nucleate boiling at z_{MHF}. For average boiling curves (q versus $\Delta \bar{T}_{w,e}$), there is smooth transition at MHF from film to nucleate boiling as z_{MHF} moves downstream towards the exit. The slope of the boiling curve in this transition region is near-zero.

Table 13
Parameter ranges of acceptable local minimum heat flux (MHF) and local re-wet wall temperature (RT) data.

Reference	Acceptable MHF data	Tube dimensions			Operating and Inlet Conditions [b]			MHF Conditions			Re-wet Conditions			Remarks
		D x 10^3 [m]	L_H/D	P x 10^{-6} [N m^{-2}]	G [kg m^{-2} s^{-1}]	q_{MHF} x 10^{-3} [W m^{-2}]	q_{max} x 10^{-3} [W m^{-2}]	$x_{e,in}$	z_{MHF} x 10^3 [m]	$x_{e,MHF}$	$T_{w,rewet}$ [K]	$\Delta T_{w,e,rewet}$ [K]	$h_{tp,e,rewet}$ [W m^{-2} K^{-1}]	
Liquid Helium														
(a) Vertical Upflow														
Panek *et al.* [*,+] [69]	17	6.35	0.79	0.04	3.97	4.01	7.59	0	0.11	0	–	–	–	OFHC Copper Tube CHF type [c] at q_{max}: DNB Film Boiling Regime [d]: IAFB
		6.35	0.79	0.1	63.16	5.12	9.72	0	2.68	0.01	–	–	–	
Hildebrandt [*,++] [1]	1	1	20	0.08	22.3	1.15	1.81	0	13.17	0.12	4.93	0.95	1218.23	Silver Block, ε = 1 μm CHF type [c] at q_{max}: DNB Film Boiling Regime [d]: IAFB
		1	20	0.08	22.3	1.15	1.81	0	13.17	0.12	4.93	0.95	1218.23	
Ogata and Sato [**,++,a] [4]	2	1.09	77.98	0.11	82.52	0.16	–	0.59	56	0.67	4.49	0.16	896.69	SS Tube, t_w = 0.26 mm CHF type [e] at q_{max}: Dryout Film Boiling Regime [d]: DFFB
		1.09	77.98	0.11	92.16	0.63	–	0.92	56	0.94	5.03	0.7	973.96	
(b) Vertical Downflow														
Panek *et al.* [*,+] [69]	12	6.35	0.79	0.04	7.6	1.93	4.88	0	0.73	0	–	–	–	OFHC Copper Tube CHF type [c] at q_{max}: DNB Film Boiling Regime [d]: IAFB
		6.35	0.79	0.1	92.16	3.55	7.97	0	2.52	0.01	–	–	–	
LHe MHF data points	**32**													
Liquid Nitrogen														
(a) Vertical Upflow														
Simon *et al.* [**,++] [98]	35	12.8	23.83	0.23	182.18	62	–	0	19	0	356.7	248	163.17	Nickel Alloy Tube, t_w = 0.25 mm CHF type [e] at q_{max}: DNB Film Boiling Regime [d]: IAFB
		12.8	23.83	1.39	2374.69	152	–	0	19	0.02	524.07	429	455.09	
LN_2 MHF data points	**35**													
Total MHF data points	**67**													
Total Re-wet data points	**38**													

[*] References without z_{MHF} information. MHF location approximated to be same as z_{CHF} corresponding to q_{max} (see Fig. 17) which can be then found using the solution strategy adopted in Table 5.
[**] References with z_{MHF} information.
[+] References without local $T_{w,rewet}$ information.
[++] References with local $T_{w,rewet}$ information.
[a] Tests performed by fixing heat flux, mass velocity and varying inlet quality using pre-heater.
[b] q_{max} is maximum heat flux provided to test section before being reduced to MHF point (see Fig. 17).
[c] CHF type at q_{max} identified using solution strategy adopted in Table 5.
[d] Film boiling regime, dependent on CHF type, is identified from original references.
[e] CHF type at q_{max}, for references without q_{max} information, is identified from original references.

Table 14
New correlation for cryogen minimum heat flux (MHF) based on estimating MHF location, z_{MHF}, to be anchored at z_{CHF} corresponding to q_{max}.

Correlation	Equation	Constants
67 Data Points MAE (%) = 9.5 RMS (%) = 12.0 θ (%) = 98 ξ (%) = 100 **Fluids:** LHe, LN_2 **Flow Direction:** Vertical Upflow Vertical Downflow **Constraints** [a]**:** Either z_{MHF} or q_{max} must be known CHF type [c] at q_{max}: DNB Film Boiling Regime [c]: IAFB	Minimum Heat Flux (q_{MHF}): $\frac{q_{MHF}}{Gh_{fg}} = 0.25c_1 We_{fo,D}^{c_2} \left(\frac{\rho_f}{\rho_g}\right)^{c_3} (1-x_{e,in})^{1+c_4} \left(\frac{z_{MHF}}{D}\right)^{c_5-1}$ If z_{MHF} is unknown, evaluate $z_{MHF} = z_{CHF}$ at q_{max} [a] using solution strategy in Table 5.	$c_1 = 0.2821$ $c_2 = -0.3410$ $c_3 = -0.5381$ $c_4 = -0.3545$ $c_5 = 0.5594$

D x 10^3 [m]	P x 10^{-6} [N m^{-2}]	P_R	G [kg m^{-2} s^{-1}]	$x_{e,in}$	$We_{fo,D}$ x 10^{-3}	ρ_f/ρ_g	z_{MHF} x 10^3 [m]	$x_{e,MHF}$	α_{MHF} [b, c]	q_{MHF} x 10^{-3} [W m^{-2}]
1	0.04	0.07	3.97	0	0.01	6.55	0.11	0	0.02	0.16
12.8	1.39	0.49	2374.69	0.92	20.97	76.57	56	0.94	0.98	152

[a] q_{max} is maximum heat flux provided to test section before the heat flux is reduced to MHF point (see Fig. 17).
[b] Evaluated using Zivi's void fraction relation, $\alpha_{MHF} = [1 + (\frac{1-x_{e,MHF}}{x_{e,MHF}})(\frac{\rho_g}{\rho_f})^{2/3}]^{-1}$.
[c] 2 data points from Ogata and Sato [4] lack information on q_{max}, however, this reference alludes to a Dryout-type CHF and therefore DFFB-type film boiling regime, which is also confirmed by high values of α_{MHF}.

Table 15
Correlation for local re-wet temperature (RT) based on new minimum heat flux (MHF) correlation for cryogens.

Correlation	Equation	Constants
38 Data Points MAE (%) = 5.1 RMS (%) = 6.7 θ (%) = 100 ξ (%) = 100Fluids: LHe, LN_2 Flow Direction: Vertical Upflow Constraints [a]: Either z_{MHF} or q_{max} must be known CHF type [c] at q_{max}: DNB Film Boiling Regime [c]: IAFB	Local *Re*-wet Temperature ($T_{w,rewet}$): $\Delta T^*_{rewet} = \frac{T_{w,rewet}-T_{sat}}{T_{w,DB,g,e}-T_{sat}} = c_6 (Bo^*_{MHF})^{c_7}$ where $T_{w,DB,g,e} = T_{g,e} + \frac{q_{MHF}}{h_{DB,g,e}}$ $h_{DB,g,e} = 0.023 Re_{g,e}^{0.8} Pr_{g,e}^{0.4} \frac{k_{g,e}}{D}$ $Re_{g,e} = \frac{GDx_{e,MHF}}{\mu_{g,e}}$ and $Pr_{g,e} = \frac{\mu_{g,e} c_{p,g,e}}{k_{g,e}}$ with all thermophysical properties of vapor are evaluated at $T_{g,e}$ $x_{e,MHF} = x_{e,in} + 4 \frac{q_{MHF}}{Gh_{fg}} \frac{z_{MHF}}{D}$ Modified Boiling Number at MHF, Bo^*_{MHF}: $Bo^*_{MHF} = \frac{x_{e,MHF}-x_{e,in}}{1-x_{e,in}}$ Minimum Heat Flux (q_{MHF}) from Table 14	$c_6 = 0.1634$ $c_7 = 0.1427$

D x 10^3 [m]	P x 10^{-6} [N m^{-2}]	P_R	G [kg m^{-2} s^{-1}]	$x_{e,in}$	z_{MHF} x 10^3 [m]	$x_{e,MHF}$	α_{MHF} [b, c]	q_{MHF} x 10^{-3} [W m^{-2}]	$T_{w,rewet}$ [K]	$\Delta T_{w,e,rewet}$ [K]
1	0.08	0.07	22.30	0	13.17	0	0.02	0.16	4.49	0.16
12.8	1.39	0.49	2374.69	0.92	56	0.94	0.98	152	524.07	429

[a] q_{max} is maximum heat flux provided to test section before the heat flux is reduced to MHF point (see Fig. 17).
[b] Evaluated using Zivi's void fraction relation, $\alpha_{MHF} = [1 + (\frac{1-x_{e,MHF}}{x_{e,MHF}})(\frac{\rho_g}{\rho_f})^{2/3}]^{-1}$.
[c] 2 data points from Ogata and Sato [4] lack information on q_{max}, however, this reference alludes to a Dryout-type CHF and therefore DFFB-type film boiling regime, which is also confirmed by high values of α_{MHF}.

and its predictive capability graphically presented in Fig. 18.

For rewet temperature (RT), the proposed functional form is based on the hypothesis that the wall temperature just before MHF should obey the physics for IAFB, which was presented in Fig. 12. This hypothesis is shown in Fig. 19. From the re-wet temperature data by Simon et al. [98] with saturated liquid inlet conditions, it is seen that for fixed z_{MHF} and q_{MHF}, $\Delta T_{w,e,rewet}$ decreases as $x_{e,MHF}$ increases. Similarly, it is also observed that for fixed z_{MHF} and $x_{e,MHF}$, $\Delta T_{w,e,rewet}$ increases as q_{MHF} increases. Both of these inferences point to an increase in $\Delta T_{w,e,rewet}$ for fixed z_{MHF} if $x_{e,MHF}$ increases and q_{MHF} decreases. Since MHF is the limiting case of IAFB as the heat flux is reduced, the LN_2 MHF data of Simon et al. [98] are mapped on a plot of normalized wall temperature ($\Delta T^*_{sat,DB}$) versus modified boiling number (Bo^*) and is checked for consistency with the trend of saturated IAFB data in Fig. 12. It is observed that both the LN_2 MHF data by Simon et al. [98] and single LHe MHF datapoint by Hildebrandt [1] undergo IAFB until MHF, therefore obeying the expected trend. Employing this hypothesis, a new correlation for local RT is constructed in Table 15,

$$T_{w,rewet} = T_{sat} + 0.16\left(T_{w,DB,g,e} - T_{sat}\right)\left(Bo^*_{MHF}\right)^{0.14}, \quad (15)$$

and its predictive capability graphically presented in Fig. 20.

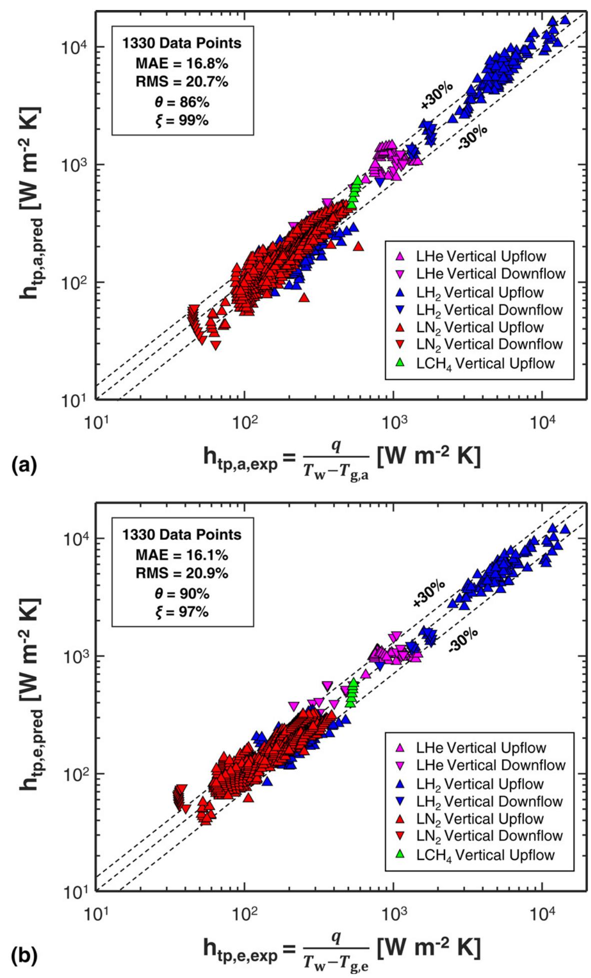

Fig. 14. Comparison of cryogen data from PU-BTPFL post-CHF HTC Database with predictions of new universal correlations for saturated ($0 \le x_e \le 1$) DFFB HTC (a) based on actual quality, x_a, actual vapor enthalpy, $h_{g,a}$, and actual vapor temperature, $T_{g,a}$, and (b) based on equilibrium quality, x_e, and equilibrium vapor temperature, $T_{g,e}$.

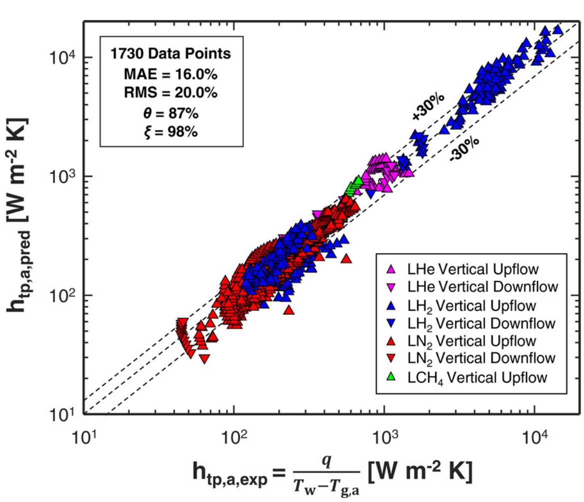

Fig. 15. Comparison of cryogen data from PU-BTPFL post-CHF HTC Database with predictions of new universal correlation for saturated and superheated DFFB HTC based on actual quality, x_a, actual vapor enthalpy, $h_{g,a}$, and actual vapor temperature, $T_{g,a}$.

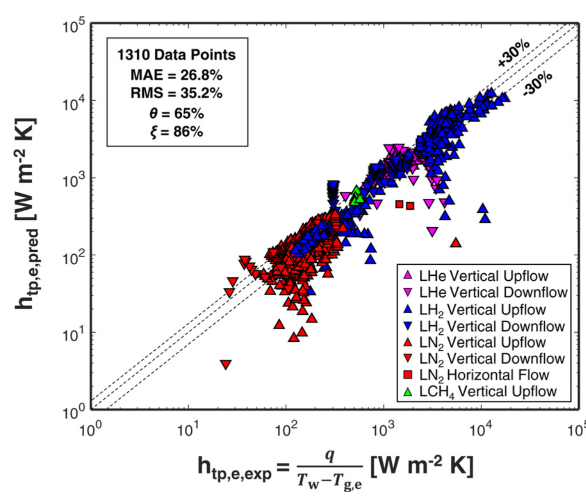

Fig. 16. Comparison of cryogen data from PU-BTPFL post-CHF HTC Database with predictions of new universal correlation for saturated and superheated (*only* LH_2) IAFB HTC based on equilibrium quality, x_e, and equilibrium vapor temperature, $T_{g,e}$.

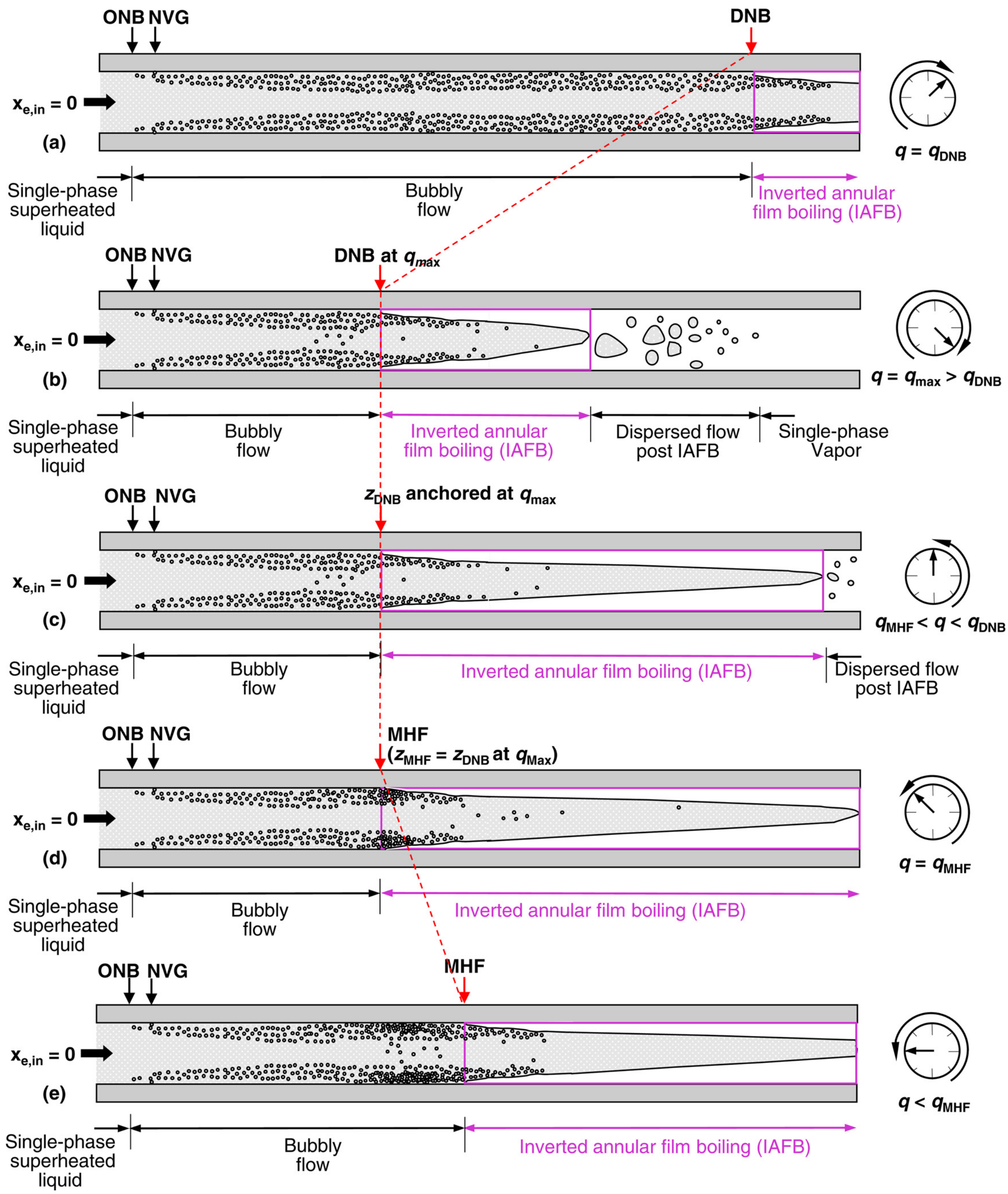

Fig. 17. Proposed hypothesis for estimating location of Minimum Heat Flux (MHF) along uniformly heated tube undergoing inverted annular film boiling (IAFB) as the flow regime transitions from film to nucleate boiling for DNB-type CHF (high G, high q, and Low L_H/D) in vertical upflow with saturated liquid inlet.

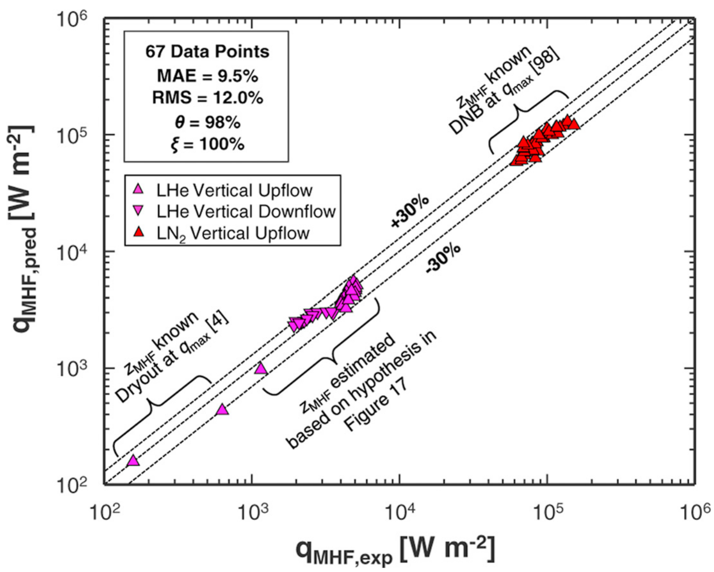

Fig. 18. Comparison of cryogen data with predictions of new minimum heat flux (MHF) correlation, estimating MHF location, z_{MHF}, anchored at z_{CHF} corresponding to q_{max}.

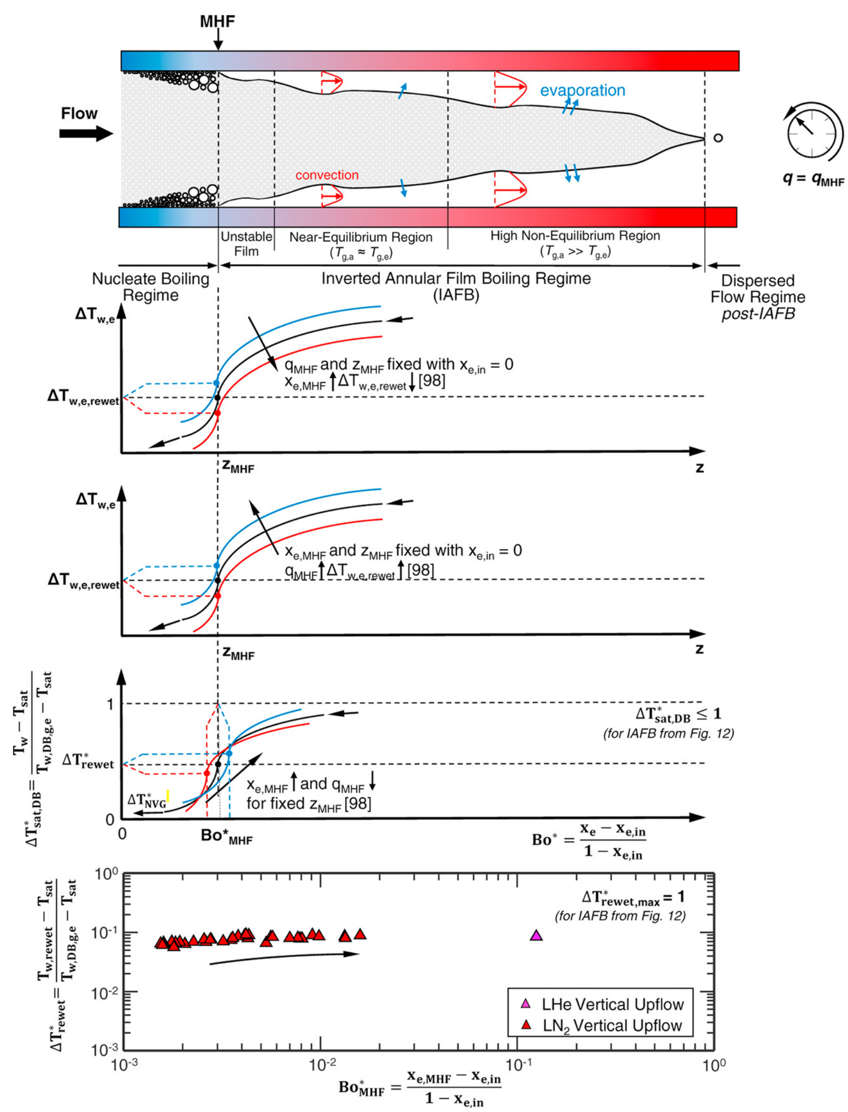

Fig. 19. Proposed hypothesis for estimating local re-wet temperature (RT) along uniformly heated tube.

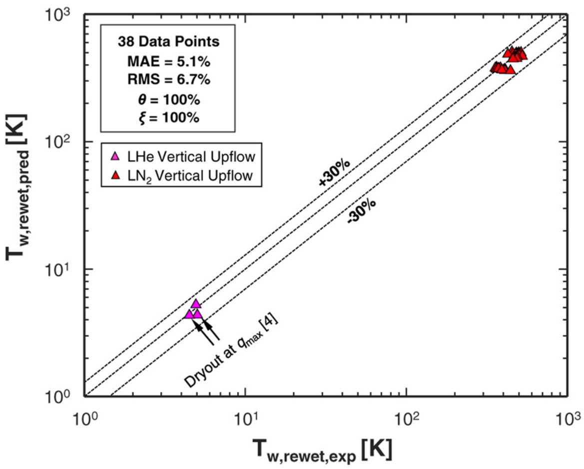

Fig. 20. Comparison of cryogen data with predictions of new local re-wet temperature (RT) based on new minimum heat flux (MHF) correlation.

5. Conclusions and Recommendations

The present study was motivated by absence of a large, reliable, error-free saturated and superheated flow film boiling heat transfer coefficient (HTC) database necessary for developing correlations as well as future analytic and computational models. An exhaustive literature search identified 1730 Dispersed Flow Film Boiling (DFFB) and 1310 Inverted Annular Film Boiling (IAFB) useful local post-CHF HTC data points for four different fluids, LHe, LH_2, LN_2, and LCH_4, which were consolidated into a post-CHF HTC database. Similar efforts were carried out to collect a relatively small Minimum Heat Flux (MHF) and local Rewet Temperature (RW) database. Using these database, new universal DFFB and IAFB local HTC correlations were constructed for saturated and superheated conditions. Similarly, new local MHF and local RT correlations were constructed. The new HTC correlations, intended specifically for cryogens, were found to provide good agreement with the data in terms of both predictive accuracy and trend.

Declaration of Competing Interest

NONE The authors declare that they have no known competing financial interests or personal relationships that could have appeared to influence the work reported in this paper.

Acknowledgment

The authors are grateful for financial support provided by the National Aeronautics and Space Administration (NASA) under grant no. 80GRC018C0055. The authors would also like to acknowledge the services provided by Purdue Libraries, especially its Interlibrary Loan (ILL) service, for helping acquire literature from across the world.

Appendix 1

Actual vapor bulk temperature derivation for DFFB

Local enthalpy, h, at any axial location z along the test section can be evaluated using inlet enthalpy, h_{in}, global operating conditions, q and G, and test section diameter, D, using a simple energy balance. Neglecting axial pressure variations, the local enthalpy can be determined from

$$h = h_{in} + 4\frac{q}{G}\frac{z}{D}. \quad \text{(A1.1)}$$

This local enthalpy is equal to both enthalpy (h_e) defined using thermodynamic equilibrium quality, x_e, and enthalpy (h_a) defined using non-equilibrium (actual) quality, x_a, respectively.

$$h = h_e = h_a, \quad \text{(A1.2)}$$

where

$$h_e = (1 - x_e)h_{f,e} + x_e h_{g,e} \quad \text{(A1.3)}$$

and

$$h_a = (1 - x_a)\left[h_{f,e} + c_{p,f,a}\left(T_{f,a} - T_{sat}\right)\right] + x_a[h_{g,e} + c_{p,g,a}(T_{g,a} - T_{sat})], \quad \text{(A1.4)}$$

where $T_{\text{f,a}}$ and $T_{\text{g,a}}$, are actual liquid and vapor temperature, respectively, and $c_{\text{p,f,a}}$ and $c_{\text{p,g,a}}$ are specific heat capacity values corresponding to $T_{\text{f,a}}$ and $T_{\text{g,a}}$, respectively.

Substituting Eq. (A1.3) and Eq. (A1.4) in Eq. (A1.2), the general form for actual vapor bulk temperature, $T_{\text{g,a}}$, is found as,

$$T_{g,a} = T_{sat} + \frac{(x_e - x_a)}{x_a}\frac{h_{fg}}{c_{p,g,a}} - \frac{(1 - x_a)}{x_a}\frac{c_{p,f,a}}{c_{p,g,a}}\left(T_{f,a} - T_{sat}\right). \quad \text{(A1.5)}$$

As indicated earlier, dispersion of fine evaporating liquid droplets at saturated and superheated conditions for post-CHF dispersed flow film boiling (DFFB) allows assumption that liquid will maintain saturation temperature (i.e., $T_{\text{f,a}} = T_{\text{sat}}$). This simplifies Eq. (A1.5) for both saturated ($0 \le x_e \le 1$) and superheated ($x_e > 1$) dispersed flow film boiling, resulting in the following relation for actual vapor bulk temperature,

$$T_{g,a} = T_{sat} + \frac{(x_e - x_a)}{x_a}\frac{h_{fg}}{c_{p,g,a}}, \quad \text{(A1.6)}$$

which can be solved iteratively using the relation $c_{\text{p,g,a}} = f(P, T_{\text{g,a}})$.

Alternatively, Eq. (A1.6) can be written in terms of actual vapor enthalpy using the relation

$$h_{g,a} = h_{g,e} + c_{p,g,a}(T_{g,a} - T_{sat}) = h_{g,e} + \frac{(x_e - x_a)}{x_a}h_{fg}, \quad \text{(A1.7)}$$

which can be solved to evaluate $T_{\text{g,a}}$ using the relation $T_{\text{g,a}} = f(P, h_{\text{g,a}})$.

Re-arranging Eq. (A1.7) yields

$$x_a = \frac{x_e}{1 + \left(\frac{h_{g,a} - h_g}{h_{fg}}\right)}. \quad \text{(A1.8)}$$

Equation (A.1.8) is identical to one arrived at by Forslund and Rohsenow [39].

References

[1] G. Hildebrandt, Heat transfer to boiling helium-I under forced flow in a vertical tube, in: Proceedings of the 4th International Cryogenic Engineering Conference, 1972, pp. 295–300.
[2] P.J. Giarratano, R.C. Hess, M.C. Jones, in: Forced Convection Heat Transfer to Subcritical Helium I, National Bureau of Standards Report, 1973, pp. 73–322.
[3] H. Ogata, S. Sato, Critical heat flux for two-phase flow of helium I, Cryogenics 13 (1973) 610–611.
[4] H. Ogata, S. Sato, Forced convection heat transfer to boiling helium in a tube, Cryogenics 14 (1974) 375–380.
[5] B.S. Petukhov, V.M. Zhukov, V.M. Shieldcret, Investigation of heat transfer and hydrodynamics in the helium two-phase flow in a vertical channel, in: Proceedings of the Advanced Course in Heat Exchangers: Theory and Practice, ICHMT Symposium, 1981, pp. 251–262.
[6] V.P. Beliakov, V.A. Shaposhnikov, S.P. Gorbatchev, I.I. Michailov, E.D. Mikitenko, Studies on nucleate boiling crisis of helium-I in channels of superconducting magnet systems, IEEE Trans. Magn. 15 (1979) 40–45.
[7] V.I. Romanov, A.L. Sevryugin, Yu.M. Pavlov, V.I. Antipov, Investigating burnouts with helium boiling in a channel, Teploenergetika 28 (1981) 620–622.
[8] V.V. Arkhipov, S.V. Kvasnyuk, V.I. Deev, V.K. Andreev, An experimental investigation and method of calculation of critical heat loads when boiling helium in tubes, Teploenergetika 26 (1979) 27–29.
[9] V.I. Deev, V.I. Petrovichev, A.I. Pridantsev, Y.V. Gordeev, V.V. Arkhipov, V.V. Parygin, Hydraulic resistance and burnout with helium boiling in tubes, Teploenergetika 26 (1979) 45–47.

[10] V.I. Subbotin, V.I. Deev, V.V. Arkhipov, Critical heat flux in flow boiling of helium, in: Proceedings of the International Heat Transfer Conference Digital Library, 1982, pp. 357–361.
[11] V.I. Subbotin, V.I. Deev, A.I. Pridantsev, V.K. Andreev, V.V. Arkhipov, V.N. Novikov, A.N. Savin, V.V. Solodovnikov, Heat transfer and hydrodynamics in cooling channels of superconducting devices, Cryogenics 25 (1985) 261–265.
[12] B.S. Petukhov, V.M. Zhukov, S.B. Anisimov, Cryogenic liquids forced boiling heat transfer in a rotating channel, Cryogenics 26 (1986) 226–233.
[13] T.C. Core, J.F. Harkee, B. Misra, K. Sato, Heat-transfer studies, aerojet-general corporation technical document TID/SNA-164, 1959. Full record: www.osti.gov/biblio/4254640-heat-transfer-studies.
[14] C.C. Wright, H.H. Walters, Single tube heat transfer tests—Gaseous and liquid hydrogen, Wright air development center technical report 59-423, 1959. Full record: http://contrails.iit.edu/reports/5771.
[15] J.P. Lewis, J.H. Goodykoontz, J.F. Kline, Boiling heat transfer to liquid hydrogen and nitrogen in forced flow, National Aeronautics and Space Administration Technical Note D-1314, National Aeronautics and Space Administration, 1962. https://ntrs.nasa.gov/api/citations/19620005135/downloads/19620005135.pdf
[16] Y. Shirai, H. Tatsumoto, M. Shiotsu, K. Hata, H. Kobayashi, Y. Naruo, Y. Inatani, DNB heat flux on inner side of a vertical pipe in forced flow of liquid hydrogen and liquid nitrogen, Cryogenics 92 (2018) 105–117.
[17] H. Tatsumoto, Y. Shirai, M. Shiotsu, K. Hata, H. Kobayashi, Y. Naruo, Y. Inatani, T. Kato, K. Kinoshita, Forced convection heat transfer of subcooled liquid hydrogen in a small tube, Proceedings of the 23rd International Cryogenic Engineering & International Cryogenic Materials Conference (2010) 491–496.
[18] Y. Shirai, H. Tatsumoto, K. Hata, M. Shiotsu, H. Kobayashi, Y. Naruo, Y. Inatani, Preliminary study on heat transfer characteristics of liquid hydrogen for coolant of HTC superconductors, AIP Conf. Proc. 1218 (2010) 337–339.
[19] H. Tatsumoto, Y. Shirai, M. Shiotsu, K. Hata, H. Kobayashi, Y. Naruo, Y. Inatani, T. Kato, M. Futakawa, K. Kinoshita, Development of a thermal-hydraulics experimental system for high Tc superconductors cooled by liquid hydrogen, J. Phys. Conf. Ser. 234 (2010) 032056.
[20] Y. Shirai, H. Tatsumoto, M. Shiotsu, K. Hata, H. Kobayashi, Y. Naruo, Y. Inatani, K. Kinoshita, Forced flow boiling heat transfer of liquid hydrogen for superconductor cooling, Cryogenics 51 (2011) 295–299.
[21] Y. Shirai, M. Shiotsu, H. Kobayashi, T. Takegami, H. Tatsumoto, K. Hata, H. Kobayashi, Y. Naruo, Y. Inatani, K. Kinoshita, DNB heat flux in forced flow of subcooled liquid hydrogen under pressures, AIP Conf. Proc. 1434 (2012) 1067–1074.
[22] H. Tatsumoto, Y. Shirai, M. Shiotsu, K. Hata, Y. Naruo, H. Kobayashi, Y. Inatani, K. Kinoshita, Forced convection heat transfer of liquid hydrogen through a 200-mm long heated tube, Phys. Procedia 36 (2012) 1360–1365.
[23] H. Tatsumoto, Y. Shirai, M. Shiotsu, K. Hata, Y. Naruo, H. Kobayasi, Y. Inatani, Forced convection heat transfer of saturated liquid hydrogen in vertically–mounted heated pipes, AIP Conf. Proc. 1573 (2014) 44–51.
[24] T. Matsumoto, Y. Shirai, M. Shiotsu, K. Fujita, Y. Iwami, Y. Naruo, H. Kobayashi, S. Nonaka, Y. Inatani, Film boiling heat transfer properties of liquid hydrogen flowing inside of heated pipe, IOP Conf. Ser. Mater. Sci. Eng. 502 (2019) 012090.
[25] H. Tatsumoto, Y. Shirai, M. Shiotsu, K. Hata, Y. Naruo, H. Kobayashi, Y. Inatani, K. Kinoshita, Forced convection heat transfer of subcooled liquid hydrogen in horizontal tubes, AIP Conf. Proc. 1434 (2012) 747–754.
[26] H. Tatsumoto, Y. Shirai, K. Hata, T. Kato, M. Futakawa, M. Shiotsu, Forced convection heat transfer of subcooled liquid nitrogen in a vertical tube, In. J. Phys. Conf. Ser. 234 (2010) 032057.
[27] H. Tatsumoto, Y. Shirai, K. Hata, T. Kato, M. Shiotsu, Forced convection heat transfer of subcooled liquid nitrogen in horizontal tube, AIP Conf. Proc. 985 (2008) 665–672.
[28] J. Van Noord, A heat transfer investigation of liquid and two-phase methane. NASA Tech. Memo. 2010-216918, 2010. Full record: https://ntrs.nasa.gov/citations/20110000533.
[29] A. Trejo, M.J. Galvan, A.G. Trujillo, A.R. Choudhuri, Experimental investigation of liquid methane convection and boiling in rocket engine cooling channels, in: Proceedings of the 50th AIAA/ASME/SAE/ASEE Joint Propulsion Conference, 2014, pp. 4007–4022.
[30] A. Trejo, C. Garcia, A. Choudhuri, Experimental investigation of transient forced convection of liquid methane in a channel at high heat flux conditions, Exp. Heat Transf. 29 (2016) 97–112.
[31] A. Trejo, A. Trujillo, M. Galvan, A. Choudhuri, J.C. Melcher, J.J. Bruggemann, Experimental investigation of methane convection and boiling in rocket engine cooling channels, J. Thermophys. Heat Transf. 30 (2016) 937–945.
[32] E.W. Lemmon, I.H. Bell, M.L. Huber, M.O. McLinden, NIST Standard Reference Database 23: Reference Fluid Thermodynamic and Transport Properties-REFPROP, Version 10.0, Standard Reference Data Program, NIST, Gaithersburg, 2018.
[33] S. Mukherjee, I. Mudawar, Pumpless loop for narrow channel and micro-channel boiling from vertical surfaces, J. Electron. Packag. 125 (2003) 431–441.
[34] M.E. Johns, I. Mudawar, An ultra-high power two-phase jet-impingement avionic clamshell module, J. Electron. Packag. 118 (1996) 264–270.
[35] G. Liang, I. Mudawar, Review of pool boiling enhancement with additives and nanofluids, Int. J. Heat Mass Transf. 124 (2018) 423–453.
[36] G. Liang, I. Mudawar, Review of single-phase and two-phase nanofluid heat transfer in macro-channels and micro-channels, Int. J. Heat Mass Transf. 136 (2019) 324–354.
[37] H. Zhang, I. Mudawar, M.M. Hasan, Experimental and theoretical study of orientation effects on flow boiling CHF, Int. J. Heat Mass Transf. 45 (2002) 4463–4478.
[38] U.H. von Glahn, J.P. Lewis, Nucleate-and film-boiling studies with liquid hydrogen, Adv. Cryog. Eng. 5 (1960) 262–269.
[39] R.P. Forslund, W.M. Rohsenow, Thermal Non-Equilibrium in Dispersed Flow Film Boiling in a Vertical Tube, 44, Massachusetts Institute of Technology, Heat Transfer Laboratory, 1966 Technical Report.
[40] S.A. Klein, EES – Engineering Equation Solver, version 10.834-3D, [2020-05-27]. F-Chart Software, Full Record: https://fchartsoftware.com/assets/downloads/faq.pdf.
[41] S. Miwa, T. Hibiki, Inverted annular two-phase flow in multiphase flow systems, Int. J. Heat Mass Transf. 186 (2022) 122340.
[42] W.H. McAdams, in: Heat Transmission, 2nd ed, McGraw-Hill Book Co, New York, 1942, p. 168.
[43] L.A. Bromley, N.R. LeRoy, J.A. Robbers, Heat transfer in forced convection film boiling, Ind. Eng. Chem. 45 (1953) 2639–2646.
[44] R.S. Dougall, Film Boiling on the Inside of Vertical Tubes with Upward Flow of the Fluid at Low Qualities, Massachusetts Institute of Technology, 1963.
[45] D.C. Groeneveld, Post-Dryout Heat Transfer at Reactor Operating Conditions, Atomic Energy of Canada Ltd., 1973 Report AECL-4513.
[46] W.F. Laverty, W.M. Rohsenow, Film Boiling of Saturated Liquid Flowing Upward Through a Heated Tube: High Vapor Quality Range, Massachusetts Institute of Technology, Heat Transfer Laboratory, 1964 Technical Report 9857-32.
[47] R.P. Forslund, W.M. Rohsenow, Dispersed flow film boiling, J. Heat Transf. 90 (1968) 399–407.
[48] S.J. Hynek, Forced-Convection, Dispersed-Flow Film Boiling, Massachusetts Institute of Technology, 1969.
[49] A.F. Varone, W.M. Rohsenow, Post dryout heat transfer prediction, Nucl. Eng. Des. 95 (1986) 315–327.
[50] M.M. Shah, Comprehensive correlation for dispersed flow film boiling heat transfer in mini/macro tubes, Int. J. Refrig. 78 (2017) 32–46.
[51] A.G. Monroe, H.A.S. Bristow, J.E. Newell, Heat transfer to boiling liquids at low temperatures and elevated pressures, J. Appl. Chem. 2 (1952) 613–624.
[52] L.E. Dean, L.M. Thompson, K.R. Stehling, T.F. Reinhardt, W.M. Smith, Heat Transfer Characteristics of Liquid Nitrogen, Bell Aircraft Corporation, 1955 Report No. 56-982-035.
[53] H.H. Walters, Single-tube heat transfer tests with liquid hydrogen, Adv. Cryog. Eng. 6 (1961) 509–516.
[54] J.H. Jones, M. Altman, Two-phase flow and heat transfer for boiling liquid nitrogen in horizontal tubes, Chem. Eng. Prog. Symp. Ser. 61 (1965) 205–212.
[55] J.C. Burke, A.H. Rawdon, An experimental study of heat transfer to two-phase film-boiling nitrogen, in: Proceedings of the ASME-AIChE Heat Transfer Conference and Exhibit 65-HT-37, 1965, pp. 1–9.
[56] M. Jergel, R. Stevenson, Static heat transfer to liquid helium in open pools and narrow channels, Int. J. Heat Mass Transf. 14 (1971) 2099–2107.
[57] A.E. Bergles, W.D. Fuller, S.J. Hynek, Dispersed flow film boiling of nitrogen with swirl flow, Int. J. Heat Mass Transf. 14 (1971) 1343–1354.
[58] A.E. Bergles, W.D. Fuller, S.J. Hynek, Influence of swirl flow on heat transfer to nitrogen in dispersed-flow film boiling, Adv. Cryog. Eng. 16 (1971) 426–434.
[59] O.C. Iloeje, D.N. Plummer, W.M. Rohsenow, Transition from Film Boiling to Nucleate Boiling in Forced Convection Vertical Flow, Massachusetts Institute of Technology, Heat Transfer Laboratory, 1972 Technical Report DSR 72718-78.
[60] M.C. Jones, W.W. Johnson, Heat transfer and flow of helium in channels–practical limits for applications in superconductivity, National Bureau of Standards Technical Note, 675, U.S. Department of Commerce, National Bureau of Standards, 1976. https://www.google.com/books/edition/Heat_Transfer_and_Flow_of_Helium_in_Chan/MBZj9K6cLQ8C?hl=en&gbpv=0
[61] P.J. Giarratano, R.C. Hess, M.C. Jones, Forced convection heat transfer to subcritical helium I, Adv. Cryog. Eng. 19 (1995) 404–416.
[62] V.A. Grigor'ev, V.I. Antipov, Y.M. Pavlov, A.V. Klimenko, Experimental investigation of heat transfer with boiling of nitrogen and helium in tubes, Teploenergetika 24 (1977) 11–14.
[63] V. Mohr, R. Runge, in: Forced Convection Boiling of Neon in Horizontal Tubes, Hemisphere Publishing Corporation, New York, 1977, pp. 307–343.
[64] A.A. Kurilenko, S.K. Dymenko, Heat transfer in plug regime of film boiling of hydrogen in pipes, J. Eng. Phys. 40 (1981) 341–345.
[65] B.S. Petukhov, V.M. Zhukov, V.M. Shieldcret, Investigation of heat transfer and hydrodynamics in the helium two-phase flow in a vertical channel, in: Proceedings of the Advanced Course in Heat Exchangers: Theory and Practice, ICHMT Symposium, 1981, pp. 251–262.
[66] V.V. Klimenko, M.V. Fyodorov, Y.A. Fomichyov, Channel orientation and geometry influence on heat transfer with two-phase forced flow of nitrogen, Cryogenics 29 (1989) 31–36.
[67] J.M. Roman, G.R. Karr, Correlation for liquid oxygen (LOX) film boiling data, Adv. Cryog. Eng. 37 (1992) 203–208.
[68] P. Bredy, D. Neuveglise, M.X. Francois, C. Meuris, R. Duthil, Test facility for helium I two phase flow study, Cryogenics 34 (1994) 361–364.
[69] J. Panek, X. Huang, S.W. Van Sciver, Localized heat transfer to vertical forced flow two-phase helium, Adv. Cryog. Eng. 41 (1996) 173–177.
[70] H. Umekawa, M. Ozawa, Dryout and post-dryout heat transfer in a natural circulation loop of liquid nitrogen, Heat Transf. Jpn. Res. 26 (1997) 449–458.
[71] L. Benkheira, B. Baudouy, M. Souhar, Heat transfer characteristics of two-phase He I (4.2K) thermosiphon flow, Int. J. Heat Mass Transf. 50 (2007) 3534–3544.
[72] S.L. Qi, P. Zhang, R.Z. Wang, L.X. Xu, Flow boiling of liquid nitrogen in micro–tubes: part II–heat transfer characteristics and critical heat flux, Int. J. Heat Mass Transf. 50 (2007) 5017–5030.

[73] R. Yun, J.S. Hwang, J.T. Chung, Y. Kim, Flow boiling heat transfer characteristics of nitrogen in plain and wire coil inserted tubes, Int. J. Heat Mass Transf. 50 (2007) 2339–2345.
[74] P. Zhang, X. Fu, Two-phase flow characteristics of liquid nitrogen in vertically upward 0.5 and 1.0mm micro-tubes: visualization studies, Cryogenics 49 (2009) 565–575.
[75] X. Fu, P. Zhang, C.J. Huang, R.Z. Wang, Bubble growth, departure and the following flow pattern evolution during flow boiling in a mini-tube, Int. J. Heat Mass Transf. 53 (2010) 4819–4831.
[76] D. Deng, S.W. Xie, X.D. Li, R.S. Wang, Flow boiling heat transfer of liquid nitrogen in heated U-tubes, J. Heat Transf. 136 (2014) 024501.
[77] S. Mustafi, High Reynolds number Vertical Up-Flow Parameters For Cryogenic Two-Phase Helium I, University of Maryland, 2014 Ph.D. Thesis.
[78] K. Yoneda, Y. Shirai, M. Shiotsu, Y. Oura, Y. Horie, T. Matsuzawa, H. Shigeta, H. Tatsumoto, K. Hata, Y. Naruo, H. Kobayashi, Y. Inatani, Forced flow boiling heat transfer properties of liquid hydrogen for manganin plate pasted on one side of a rectangular duct, Phys. Procedia 67 (2015) 637–642.
[79] X. Fang, A.M. Sudarchikov, Y. Chen, A. Dong, R. Wang, Experimental investigation of saturated flow boiling heat transfer of nitrogen in a macro-tube, Int. J. Heat Mass Transf. 99 (2016) 681–690.
[80] X. Liu, X. Chen, Q. Zhang, S. Wang, Y. Hou, L. Chen, Investigation on CHF of saturated liquid nitrogen flow boiling in a horizontal small channel, Appl. Therm. Eng. 125 (2017) 1025–1036.
[81] T. An, Y. Wang, W.Q. Liu, Experimental investigation of heat transfer characteristics of liquid nitrogen flow boiling in a mini-channel, in: Proceedings of the International Heat Transfer Conference Digital Library, 2018, pp. 6479–6485.
[82] B.C. Zhang, Q.L. Li, Y. Wang, J.Q. Zhang, J. Song, F.C. Zhuang, Experimental investigation of nitrogen flow boiling heat transfer in a single mini-channel, J. Zhejiang Univ. Sci. A 21 (2020) 147–166.
[83] R.C. Hendricks, R.W. Graham, Y.Y. Hsu, R. Friedman, Experimental heat transfer and pressure drop of film boiling liquid hydrogen flowing through a heated tube, National Aeronautics and Space Administration Technical Note D-765, National Aeronautics and Space Administration, 1961. https://apps.dtic.mil/sti/pdfs/AD0255524.pdf
[84] R.C. Hendricks, R.W. Graham, Y.Y. Hsu, R. Friedman, Experimental heat-transfer results for cryogenic hydrogen flowing in tubes at subcritical and supercritical pressures to 800 pounds per square inch absolute, National Aeronautics and Space Administration Technical Note D-3095, National Aeronautics and Space Administration, 1966. https://ntrs.nasa.gov/citations/19660011645
[85] M.R. Glickstein, R.H. Whitesides, Forced-convection nucleate and film boiling of several aliphatic hydrocarbons, in: Proceedings of the ASME-AIChE Heat Transfer Conference and Exhibit 67-HT-7, 1967, pp. 1–8.
[86] S.S. Papell, Buoyancy effects on forced-convective boiling, in: Proceedings of the ASME-AIChE Heat Transfer Conference and Exhibit 67-HT-63, 1967, pp. 1–9.
[87] C. Peroulias, L.H. Pidcoke, S.H. Schwartz, D.E. Mussell, Boiling oxygen experimental studies in an electrically heated tube, in: Proceedings of the 24th Joint Propulsion Conference, 1988 AIAA-88-2842.
[88] B. Xu, Y. Shi, D. Chen, Z. Yu, Heat transfer characteristics during flow boiling of liquid nitrogen in vertical tube, CIESC J. 65 (2014) 460–467.
[89] Y. Shirai, M. Shiotsu, T. Matsumoto, H. Kobayashi, Y. Naruo, S. Nonaka, Y. Inatani, Heat transfer characteristics of liquid hydrogen flowing inside of a vertical heated pipe under quasi-stationary heat input, Cryogenics 113 (2021) 103230.
[90] F.W. Dittus, L.M.K. Boelter, Heat transfer in automobile radiators of the tubular type, Int. Comm. Heat Mass Transf. 12 (1985) 3–22.
[91] V. Ganesan, R. Patel, J. Hartwig, I. Mudawar, Universal critical heat flux (CHF) correlations for cryogenic flow boiling in uniformly heated tubes, Int. J. Heat Mass Transf. 166 (2021) 120678.
[92] S.M. Zivi, Estimation of steady-state steam void-fraction by means of the principle of minimum entropy production, ASME J. Heat Transf. 86 (1964) 247–252.
[93] H. Umekawa, M. Ozawa, T. Yano, Boiling two-phase heat transfer of LN_2 downward flow in pipe, Exp. Therm. Fluid. Sci. 26 (2002) 627–633.
[94] S.S. Papell, Film boiling of cryogenic hydrogen during upward and downward flow, National Aeronautics and Space Administration Technical Memorandum X-67855, National Aeronautics and Space Administration, 1971. https://ntrs.nasa.gov/citations/19710018390
[95] Q. Zhang, J. Chen, J. Li, J. Cao, L. Chen, Y. Hou, Experimental study on saturated flow boiling heat transfer of nitrogen in a small-diameter horizontal heated tube, Exp. Therm. Fluid. Sci. 86 (2017) 257–271.
[96] S.S. Papell, Buoyancy effects on liquid nitrogen film boiling in vertical flow, National Aeronautics and Space Administration Technical Memorandum X-52808, National Aeronautics and Space Administration, 1970. https://ntrs.nasa.gov/citations/19700020670
[97] I.L. Yarmak, V.M. Zhukov, Forced liquid helium flow transient heat transfer in a narrow channel under step heat flux, Cryogenics 32 (1992) 729–736.
[98] F.F. Simon, S.S. Papell, R.J. Simoneau, Minimum film-boiling heat flux in vertical flow of liquid nitrogen, National Aeronautics and Space Administration Technical Note D-4307, National Aeronautics and Space Administration, 1968. https://ntrs.nasa.gov/api/citations/19680007214/downloads/19680007214.pdf.